

A MEASUREMENT OF THE VALUE OF THE HUBBLE CONSTANT FROM THE X-RAY PROPERTIES AND THE SUNYAEV-ZEL'DOVICH EFFECT OF ABELL 665

M. BIRKINSHAW,¹ J. P. HUGHES,¹ AND K. A. ARNAUD²

Received 1991 January 7; accepted 1991 April 17

ABSTRACT

A comparison of the X-ray properties and the Sunyaev-Zel'dovich effect for a cluster of galaxies may be used to measure the distance of the cluster, and hence the Hubble constant. We have applied this method to the rich cluster Abell 665 using IPC, HRI, and MPC data from the *Einstein Observatory*, LAC data from the *Ginga* satellite, and Sunyaev-Zel'dovich data from the OVRO 40 m telescope.

The X-ray and Sunyaev-Zel'dovich effect data are consistent in their description of the cluster gas and may be fitted by a simple isothermal β -model with $\beta \approx 0.66$, cluster core radius ≈ 1.6 , and gas temperature ≈ 8.2 keV. The relative normalizations of the X-ray and Sunyaev-Zel'dovich effect data then lead to an estimated Hubble constant $H_0 = 40 \pm 9$ km s⁻¹ Mpc⁻¹ if only the random errors are included. When the possible systematic errors (which are most important if they are present in the Sunyaev-Zel'dovich data) are added in quadrature, the range of possible values of the Hubble constants expands to $(40 \text{ to } 50) \pm 12$ km s⁻¹ Mpc⁻¹.

The most immediate improvements in the error in this estimate for the Hubble constant would be produced by setting better limits on the zero level of the Sunyaev-Zel'dovich effect data (involving extensive observation), and by improved X-ray observations of the cluster, possibly with *ROSAT*, *Astro-D*, and *AXAF*. However, systematic errors associated with the unknown detailed thermal and density structures of the gas (clumping and low-surface brightness structures) provide limits to the accuracy of the method in principle.

Subject headings: cosmology — galaxies: clustering — galaxies: intergalactic medium — galaxies: X-rays

1. INTRODUCTION

The Hubble constant is usually measured with the aid of a number of distance indicators of overlapping applicability which allow the ascent of the cosmic distance ladder (see the review of Tully 1988). Two canonical distance scales, characterized by values of the Hubble constant ≈ 50 and 100 km s⁻¹ Mpc⁻¹, have resulted. Recent work using the infrared magnitude/H I velocity width correlation tends to favor the larger Hubble constant (Aaronson et al. 1986), as does work using look-alike galaxies at different distances (de Vaucouleurs & Corwin 1986). On the other hand, the use of Type I supernovae, the brightest stars, and H II regions as distance indicators, as summarized by Tammann & Sandage (1983), has led to the smaller Hubble constant.

These conventional approaches to the Hubble constant suffer from the difficulty of relating the properties of nearby distance indicators, for which relatively precise distances are known, to the properties of (different) indicators in galaxies at a sufficient redshift that they are unaffected by the local supercluster. An alternative approach to distance measurement is provided by "astrophysical" methods: where a phenomenon observed at a substantial redshift is interpreted in such a way as to provide a distance for the object sustaining it. Several of these methods use the properties of supernovae (Bartel 1985; Branch 1985), and tend to support a small Hubble constant. Lynden-Bell (1977) proposed a method based upon a light echo interpretation of superluminal motions in active galactic nuclei, and derived $H_0 \approx 100$ km s⁻¹ Mpc⁻¹, but this explana-

tion for superluminal motions is no longer in favor. Finally, a number of variations on a method that uses the properties of the hot atmosphere in a cluster of galaxies have been suggested (Gunn 1978; Silk & White 1978; Birkinshaw 1979; Cavaliere, Danese, & De Zotti 1979; Krolik & Raymond 1988). In this paper we shall use X-ray and Sunyaev-Zel'dovich effect data for the rich cluster of galaxies Abell 665 to deduce H_0 using this last technique.

The basis of the method is that the Sunyaev-Zel'dovich effect of a cluster (the reduction in the brightness of the microwave background radiation produced by inverse-Compton scattering of the radiation by electrons in the cluster atmosphere) and the thermal bremsstrahlung X-ray flux from the cluster scale differently with the mean gas density and size of the cluster. The Sunyaev-Zel'dovich effect is proportional to the product of the inverse-Compton scattering depth through the cluster and the mean energy change of a scattered photon, and hence scales as

$$\Delta T_{RJ} \propto \overline{n_e T_e} L, \quad (1.1)$$

where L is the line-of-sight length in the atmosphere, and $\overline{n_e T_e}$ is the average product of electron concentration and temperature along that line of sight. The total X-ray flux from the cluster scales as

$$S_X \propto V \frac{\overline{n_e n_p T_e^{1/2}}}{D_L^2}, \quad (1.2)$$

approximately, where this average is over the volume V of the cluster and D_L is its luminosity distance. If the thermal and density structures of the cluster and the metallicity of the cluster gas are understood, then the electron and proton concentrations n_e and n_p ($\propto n_e$) can be eliminated between these equations. The volume $V \propto L \theta^2 D_A^2$, where D_A is the angular diameter distance and θ is the angular size of the cluster, so

¹ Harvard-Smithsonian Center for Astrophysics, 60 Garden Street, Cambridge, MA 02138.

² Code 666, Goddard Space Flight Center, Greenbelt, MD 20771, and Astronomy Program, University of Maryland, College Park, MD 20742.

that the *linear* scale of the cluster,

$$L \propto \Delta T_{R_I}^2 S_X^{-1} \bar{T}_e^{-3/2}, \quad (1.3)$$

and D_A may be estimated from L/θ if the shape of the cluster is known. When combined with the cluster redshift, this yields the Hubble constant (with some dependence on q_0).

It will be seen that for this method to be used effectively,

1.—The mean electron temperature of the atmosphere, \bar{T}_e , must be known accurately. This requires a good X-ray spectrum for the cluster,

2.—The three-dimensional density and thermal structure of the cluster must be known. This requires fitting models or finding deconvolutions and deprojections of X-ray and Sunyaev-Zel'dovich effect maps of the cluster, or resolved X-ray spectroscopy of the atmosphere, and

3.—The Sunyaev-Zel'dovich effect and X-ray emission must be free from contamination from other sources.

If the necessary data are available, then this method has a number of advantages. First, the physical basis for the method is simple—it relies on the properties of a fully ionized gas, held nearly in hydrostatic equilibrium in the gravitational potential well of the cluster of galaxies. Second, it may be applied at large cosmological distances directly, without the intervening chain of distance estimators in the usual distance ladder. X-ray emission and the Sunyaev-Zel'dovich effect have been found from at least one cluster of galaxies at a redshift exceeding 0.5 (White, Silk, & Henry 1981; Birkinshaw, Gull, & Moffet 1981; Birkinshaw, Gull, & Hardebeck 1984). Third, the method may be applied to each cluster of galaxies as an individual—the evolutionary peculiarities of a distant cluster need not affect the application of the method, as long as the physical state of the gas bound to that cluster is understood. Of course, if the cluster is structurally irregular, the difficulty in applying the method may become extreme. Finally, the problem is, formally, overdetermined if the full range of observable quantities has been accurately measured for a cluster and spherical symmetry is valid. The method therefore provides an internal consistency check. In practice, this full data set is not available for any single cluster—and the effectiveness of the method is thereby reduced.

The principal disadvantage of the method is that since the X-ray and Sunyaev-Zel'dovich structures depend on different functions of the density and temperature of the gas, the largest contributions to these effects come from physically different parts of the atmosphere. The X-ray flux is dominated by emission from the highest density parts of the atmosphere, because of the n_e^2 factor in equation (1.2), while the Sunyaev-Zel'dovich effect is produced in lower density regions of the cluster, where the path lengths are longer (eq. [1.1]). Thus, it is important that the three-dimensional structure of the cluster atmosphere is known, and that the density distribution smoothly relates the properties of gas in those parts of the cluster that produce the Sunyaev-Zel'dovich effect and the X-ray emission. This would not be the case if, for example, the X-ray-emitting gas lies within a shock around the cluster core, such as might be produced by a strong matter infall, while the Sunyaev-Zel'dovich effect is dominated by the gas outside the shocked core. In terms of the calculation performed here, we shall assume that the structure of the cluster can be characterized by a simple thermal and density model, and then we shall determine the model-dependence of the solution for H_0 .

Several previous attempts have been made to apply this method—generally they have encountered difficulties in mea-

suring the temperature of the atmosphere. Birkinshaw (1979) suggested modeling the cluster potential to avoid this problem—however, this approach requires an accurate measurement of the velocity dispersion of a cluster at redshift ≈ 0.2 , the inference of a good mass model for the cluster, and excellent knowledge of the extent to which the potential well is filled with gas. A better approach is clearly to make a direct measurement of the temperature by X-ray spectroscopy, but no good X-ray temperature was available for those clusters for which the Sunyaev-Zel'dovich effect had been measured when White & Silk (1980) and Boynton et al. (1982) attempted to use the method for Abell 576 and Abell 2218.

As we shall show, the situation has now improved somewhat, at least for the cluster Abell 665 (and possibly Abell 2218; McHardy et al. 1990). Recent Sunyaev-Zel'dovich data (Birkinshaw et al. 1991) have measured the angular structure of the effect along a north-south line near the cluster center. The *Einstein* satellite obtained X-ray images of the cluster with both the Imaging Proportional Counter (IPC) and the High Resolution Imager (HRI). An X-ray spectrum is available both from the Monitoring Proportional Counter (MPC) on *Einstein* and, more recently, from the *Ginga* satellite. We have used these data to characterize the atmosphere of Abell 665 and checked their internal consistency. The results can also be used to determine which of the data used to measure H_0 are critical to an improvement in accuracy.

Abell 665 lies at redshift $z = 0.182$ (Sargent 1973; Huchra & Birkinshaw 1989, private communication) and is the richest cluster in Abell's (1958) list, with a richness class of 5. The distribution of galaxies in the cluster has been studied by Geller & Beers (1982), who find two distinct condensations in the galaxy counts. The larger of these is centered on a prominent cD galaxy, the smaller lies about 10' to the northwest of this galaxy. The distribution and luminosity function of the galaxies has been studied by Dressler (1978a, b); he finds that the cluster is somewhat less rich than its Abell class would suggest. Abell 665 was observed by the *Einstein Observatory* as a part of a major guaranteed time project concerned with the investigation of rich clusters of galaxies. Observations of the cluster in the Sunyaev-Zel'dovich effect have been made because of its richness, and because it was known that these X-ray data would be taken, and have been continued on the basis of the relative freedom from interfering radio sources in the cluster (Moffet & Birkinshaw 1989) and early reports of the presence of a substantial Sunyaev-Zel'dovich effect (Lake & Partridge 1980; Birkinshaw, Gull, & Northover 1981). Confirmations of the presence of a Sunyaev-Zel'dovich effect (at a smaller intensity than was suggested in the early publications) have been obtained using different telescopes and techniques by Birkinshaw et al. (1984) and Uson (1986).

Section 2 of this paper describes the data available on the gas content of Abell 665: X-ray imaging data from the *Einstein* satellite HRI and IPC, X-ray spectral data from the *Einstein* MPC and *Ginga*, and Sunyaev-Zel'dovich data from the OVRO 40 m telescope. In § 3 the method of analysis of these data is presented. Most simply, the X-ray and Sunyaev-Zel'dovich effect data are interpreted in terms of a single, spherical, gas cloud whose linear size can be obtained absolutely for any given model of the atmosphere. For a range of models, a variety of sizes are found, and these are combined with the angular extent of the atmosphere and the redshift of the cluster to determine the Hubble constant. Section 4 then assesses the uncertainty in this estimate by taking account of

the sampling errors in the data, the range of models that can describe the data, the possibility of other processes contributing to the X-ray emission or Sunyaev-Zel'dovich effect of the cluster, and the assumptions of a single, spherical, gas cloud. The conclusions are collected in § 5.

2. THE DATA

2.1. *The Sunyaev-Zel'dovich Effect*

Observations of the Sunyaev-Zel'dovich effect have been made over the last 10 years using the 40 m telescope of the Owens Valley Radio Observatory (OVRO). The original experiment at OVRO was undertaken at 10.6 GHz, close to the frequency of earlier work performed with the 25 m telescope at Chilbolton (Gull & Northover 1976; Birkinshaw et al. 1981): the results of the 10.6 GHz OVRO work appeared as Birkinshaw & Gull (1984). More recently observations have been made at 20.3 GHz, at which frequency the 40 m telescope is equipped with a more stable, low-noise system, and appears to be less affected by systematic errors. Some results of this work have been reported by Birkinshaw et al. (1984), Birkinshaw & Moffet (1986), and Birkinshaw (1990): the data indicate the presence of significant Sunyaev-Zel'dovich decrements in all three clusters subjected to intensive 20.3 GHz observation. One of these three clusters is Abell 665.

Observations at the OVRO 40 m telescope are made by beam-switching in azimuth. The telescope is equipped with a dual-beam system at prime focus, with the two beams offset 3:58 in azimuth to either side of the telescope center line. An observing cycle consists of (typically) 10 s with the eastern beam on source, 20 s with the western beam on source, then a final 10 s with the eastern beam on source again, with brief intervals for moving the telescope between the pointings. The mean antenna temperature difference between the on-source and off-source beams in each of these pointings is recorded using a Dicke switch operating at 10 Hz and a radiometer with time constant (and sampling interval) 0.5 s. Dicke switch transients are blanked out. When the results from the three pointings are combined, the result is a measurement of the sky brightness at some central location relative to the sky brightness at points $\pm 7:15$ offset from it in azimuth. As the period of observation is extended, so the offset beam locations sweep out arcs around the point under observation. The length of these "reference arcs" is determined by the range of elevations for which observations are made (constrained by the observer's desire to observe at the lowest possible air masses, and the changing gain of the telescope at high and low elevations). Further details of the method are given by Birkinshaw & Gull (1984) and Readhead et al. (1989).

The data on Abell 665 were obtained in the observing seasons from 1983 to 1987 (no data were obtained in 1987–88 because of an equipment failure) under a range of weather conditions. No systematic, weather-dependent, offset signals have been found in the data, but in good weather the data are less noisy and exhibit smaller minute-to-minute correlations than in poor weather. Only data taken during conditions of relatively good weather (when the rms noise < 5 mK) are included in the results presented here. Observations were made at the nominal (Abell 1958, as precessed by Sastry & Rood 1971) center of Abell 665, $08^{\text{h}}26^{\text{m}}12^{\text{s}}$, $+66^{\circ}04'00''$ (1950.0), and at points $\pm 2'$, $\pm 4'$, and $\pm 7'$ to either side of it in declination.

The average signal seen at each of these points, without any corrections, is shown in column 2 of Table 1. The significant

negative signals seen toward the center of the cluster are caused by the Sunyaev-Zel'dovich effect from its hot gas, but this signal is confused by the presence of radio sources near the cluster. For the point at $+65^{\circ}57'$, radio sources of 5 and 10 mJy (sources 7 and 20 in the Moffet & Birkinshaw 1989 survey of the cluster) lie in the reference arcs and bias the signal negative. For the point at $+66^{\circ}08'$, a 1 mJy source (source 14 in the Moffet & Birkinshaw survey) lies in the on-source position and biases the signal positive. To achieve the most reliable measurements of the Sunyaev-Zel'dovich effect, corrections must be made for these, and the weaker, radio sources that contaminate the data. These corrections have been made using the preferred method of Moffet & Birkinshaw (1989) on the basis of their VLA radio survey of the field. That is, any 40 s data sample that is contaminated in its reference arcs at a level > 0.1 mK is excluded from the data set, and other data samples are corrected for the residual source contribution in the reference arcs. The data are also corrected for the (positive) contribution of any source near the central point observed. This method ensures that large and uncertain source corrections in the reference arcs do not unduly affect the results. Little can be done about sources near the points under study, however—errors in their flux densities can cause serious systematic errors. Of the seven points observed in Abell 665, only the point at $+66^{\circ}08'$ is contaminated by such a source at a level greater than $50 \mu\text{K}$. The corrected measurements of the Sunyaev-Zel'dovich effect given in column 3 of Table 1 are therefore not strongly dependent on the source corrections assumed.

The ultimate limitation on the precision of these Sunyaev-Zel'dovich effect data is set not by the level of sampling errors, but rather by the residual systematic errors in the data. Several possible sources of systematic error have been considered in estimating the maximum residual effects given in Table 1:

1.—An error in the zero level of the observation, caused, perhaps, by spillover power from the telescope, by parasitic signals which depend on the times of day or the elevation ranges over which Abell 665 was observed, or by peculiar weather conditions during the observations and a beam-beam asymmetry in the twin-beam system. The level of this systematic signal has been estimated from the measured brightness temperatures of points 7' north and south of the nominal cluster center (after subtraction of the Sunyaev-Zel'dovich effect profile implied by the best-fitting X-ray model: at the ends of the scan this profile signal is less than about 10% of the central Sunyaev-Zel'dovich effect because of the efficiency of the beam-switching technique in reducing the parallactic-angle-averaged signal at off-center points in the cluster), and from the brightness temperature of a point 12^{h} distant in (1950) right ascension from Abell 665, and nominally measuring the brightness of blank sky. The result for the maximum systematic error from the zero-level uncertainty is estimated to be in the range -41 to $+1 \mu\text{K}$.

2.—Errors in the flux density to brightness temperature conversion used in the corrections for radio sources near the points observed and on the reference arcs. These errors are only appreciable for the points 4' south of the nominal center of Abell 665 (for which the error is estimated to be -15 to $+15 \mu\text{K}$), and 4' north of the nominal center (where the systematic error is -30 to $+30 \mu\text{K}$). For all other points this error is less than $5 \mu\text{K}$.

3.—Errors from radio sources missing from the radio source correction, either because their spectra are unusual or because of variability over the period of observation. It is estimated

TABLE 1
SUNYAEV-ZEL'DOVICH EFFECT MEASUREMENTS

Location (B1950 coordinates) (1)	Uncorrected ΔT_{RJ} $\mu\text{K} \pm \mu\text{K}$ (2)	Corrected ΔT_{RJ} $\mu\text{K} \pm \mu\text{K}$ (3)	Maximum Systematic Error μK to μK (4)
08 ^h 26 ^m 12 ^s +66°11'00"	-38 ± 41	-36 ± 41	-25 to +35
+66 08 00	+55 ± 86	-25 ± 93	-29 to +40
+66 06 00	-289 ± 34	-243 ± 70	-37 to +48
+66 04 00	-318 ± 25	-301 ± 49	-42 to +52
+66 02 00	-449 ± 34	-434 ± 52	-43 to +51
+66 00 00	-271 ± 74	-282 ± 75	-42 to +50
+65 57 00	-148 ± 37	-30 ± 68	-37 to +48

NOTES.—(1) Uncorrected values of ΔT_{RJ} are those without source corrections of any kind, but with the data taken under conditions of bad weather removed. The presence of radio sources 7 and 20 (in the numbering system of the Moffet & Birkinshaw 1989 survey) in the reference arcs causes most of the source correction for the point at 65°57', and the presence of source 14 near 66°08' causes most of the correction at that point, although this is partially offset by source 20 in the reference arcs. (2) Overall zero level of these data possesses a maximum systematic error range of -41 to +1 μK , as determined by the $\pm 7'$ data and observations of a "blank-sky" region near the declination of Abell 665. (3) Overall scale of the brightness temperatures may be in error by $\pm 6\%$. (4) Systematic error is expressed as a maximum range, and the true value of the systematic offset may be thought of as a stochastic variable uniformly distributed over this range.

that no single radio source with $S_{2.0\text{GHz}} > 0.2$ mJy is missing on the reference arcs, and that no source with flux density greater than 0.1 mJy is missing near the points observed, so that the maximum systematic error from this cause is -20 to +20 μK .

4.—Where the source correction for a source near the point observed is large, the random error on that source correction may more properly be assessed as a systematic error on the brightness temperature, but for no point does this error exceed ± 10 μK . However, this estimate takes no account of source variability, which is an issue for the point at +66°08' (see § 3.2).

5.—From errors in the pointing of the 40 m telescope, which will tend to cause points near strong gradients in the Sunyaev-Zel'dovich effect, or points near the peak of the Sunyaev-Zel'dovich effect, to have incorrect brightnesses. The magnitude of this effect may be estimated from a simple theoretical model of the gas distribution and from the maximum pointing errors of the 40 m telescope ($\lesssim 0.5$). The largest systematic errors from this cause tend to arise 4' south and 2' north of the nominal cluster center, where they are less than about 50 μK .

6.—Finally, there is an error in the brightness temperature scale from the varying efficiency of the telescope at different elevations: this effect is estimated to be less than about $\pm 6\%$ of the measured brightnesses.

Most of these limits are represented in Figure 1, which displays the data for the scan through Abell 665. At each point, the cross represents the measured brightness and its statistical error (as determined directly from the data). The total systematic error from effects 2-5 is represented by the large box around the cross. It should be emphasized that these boxes represent the *maximum* estimated systematic errors: they are calculated by direct addition of the maximum positive and the maximum negative values of effects 2-5. Effect 1 is represented on Figure 1 by a range for the zero level in the plot: it can be seen that the points 7' north and south of the cluster centers lie within this range of zero level. Finally, the brightness temperature scale should be regarded as uncertain by $\pm 6\%$, as described in point 6 above.

One further correction to the observational results is necessary. When the individual results for each year of data for any one point in the scan are compared, those results should be

concordant. In fact this is not the case—the individual results are too widely dispersed about the overall average from all four years of observation. It is likely that this year-to-year discordance is caused partially by the varying condition of the telescope and receiver from year to year, for example if the pointing was of variable quality (from thermal effects, windage, etc.), and partially by variations in the systematic errors already estimated. A conservative assumption about the true variation in the data, however, requires an increase in the statistical errors to allow for this discordance. These error increases are represented on Figure 1 by the thick extensions of the error bars.

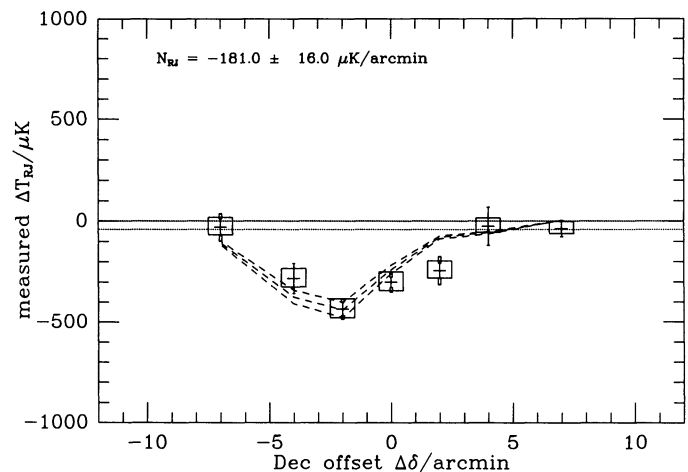


FIG. 1.—Sunyaev-Zel'dovich effect data for several points on an NS line through Abell 665. The declination offsets for each point are measured relative to the nominal cluster center (at 08^h26^m12^s, 66°04'00", 1950.0). A cross with error bars represents the microwave background radiation brightness temperature change, as measured with the OVRO 40 m telescope. The box around each cross indicates the maximum estimated additive systematic error, and the small boxes at the ends of the error bars indicate the increase in the random error suggested by the year-to-year discordance in the data. Horizontal dotted lines indicate the maximum systematic error on the overall zero level. Dashed curves represent a fit to the model of eq. (3.16) to the data, and its $\pm 1\sigma$ error, disregarding the systematic errors, and joining the fitted values at the points observed by straight line segments. Note that the brightness temperature scale is uncertain by $\pm 6\%$.

For each point, Table 1 records the mean brightness temperature, the discordance-adjusted statistical error, and an estimate of the maximum systematic error. Even if full systematic errors are assessed against each point, the data still indicate the presence of a significant, resolved, Sunyaev-Zel'dovich effect in Abell 665.

It can clearly be seen from Figure 1 that the peak Sunyaev-Zel'dovich effect in Abell 665 lies about 2' south of the nominal cluster center. The apparent asymmetry in the Sunyaev-Zel'dovich effect—the greater angular extent to the north of the peak—does not indicate a statistically significant deviation from a spherically symmetric distribution. The overall angular extent of the effect is about 5' (full width to half-maximum), significantly broader than the beamwidth of the 40 m telescope (1'.8). Note that a direct comparison of the data in Figure 1 with a smooth model atmosphere is difficult since each point in the scan represents a different weighting over the reference arcs, because of the different exposures that each point received, and because different segments of the reference arcs have been removed to avoid difficulties with radio sources. This sampling of the reference arcs is taken into account explicitly in later analysis of the data.

2.2. The X-Ray Images

X-Ray images of Abell 665 were obtained using both the imaging proportional counter (IPC) and the high resolution imager (HRI) on the *Einstein Observatory*. An ephemeris of these observations is shown in Table 2, and the characteristics of the IPC and HRI are discussed in Giacconi et al. (1979); below we summarize the details that are relevant to these observations of Abell 665.

The heart of the *Einstein Observatory* was a high-resolution, grazing-incidence, X-ray telescope. The critical energy for grazing incidence reflection from the mirrors used in the telescope was about 4.5 keV, so that photons with greater energies were absorbed rather than focused, and the effective area of the telescope decreased rapidly at energies above 4.5 keV. In consequence, it is not possible to use the data from the *Einstein* images to make accurate measurements of the temperatures of hot objects, such as clusters of galaxies (for which the temperatures are usually around 7 keV). However, the *Einstein* images provide good maps of the overall X-ray surface brightness of a cluster of galaxies, and we can use these data for Abell 665 to constrain the gas density distribution in its intracluster medium.

The IPC was a low-background, gas-filled detector with good imaging and modest spectral capabilities. The spatial resolution was about 36" (1σ) in an approximately Gaussian beam, and the energy resolution $\Delta E/E$ was about unity at 1 keV. The effective area of the IPC on the *Einstein* telescope was somewhat more than 100 cm² at 1 keV. The intrinsic background rate in orbit was about 5×10^{-4} counts s⁻¹ arcmin⁻²,

and was composed of a particle-induced background, the diffuse cosmic X-ray background, and a component due to solar X-rays scattered into the field of view by Earth's atmosphere.

The HRI was a microchannel plate detector for high-resolution imaging. The spatial resolution was limited by the mirror performance to about 4" (FWHM). The point spread function of the mirror/HRI combination has been modeled (Henry & Henriksen 1986) as a double exponential with scales of about 2" and 13". The HRI had no intrinsic spectral resolution. The background in the HRI arose mostly from residual radioactivity in the channel plates themselves; the average rate in orbit was about 4.6×10^{-3} counts s⁻¹ arcmin⁻². This higher background, coupled with its lower effective area (~ 10 cm² at 1 keV), made the HRI considerably less sensitive than the IPC to diffuse X-ray emission.

The *Einstein* IPC image of Abell 665 was constructed using pulse independent (PI) channels 5–10, which correspond to an observed energy range 0.8–3.5 keV. These PI bins were used (instead of the pulse height bins) to correct for possible temporal and spatial variations of the IPC gain. The backgrounds in the IPC (from high-energy particles, the diffuse X-ray background, and solar X-rays scattered by the upper atmosphere) can vary from observation to observation by about 20%. In addition to this variability, the different components of background have differing spatial distributions in the IPC. For example, both the diffuse cosmic and solar scattered background are vignettted by the telescope, while the particle background is not. The standard analysis system for the *Einstein* IPC uses two background maps, the DSMAP and the BEMAP, to correct for these backgrounds. The DSMAP is the sum of a large number of deep survey fields (effective exposure time of 277,922 s) with sources removed, and thus contains emission from both the particle-induced and the diffuse extragalactic components of the background. The BEMAP was constructed from data taken on the bright Earth and is dominated by the scattered and fluorescent solar X-ray background. Since Abell 665 does not come close to filling the field of view of the IPC, there is a considerable region in the image from which the background level can be reliably estimated. The background level has been subtracted using the following procedure. First, the DSMAP was subtracted from the image using the ratios of live times. The remaining background was then subtracted by scaling the counts in the BEMAP to the counts in the same region (in detector coordinates) of the image. The entire area of the detector lying more than 16' from the center of Abell 665 was used as the reference region for this comparison—there is no detectable point source or cluster diffuse emission in this area. To represent the variability of the background, this procedure was repeated with the fraction of DSMAP increased and decreased by 20%: the analysis of these two additional data sets yielded the sensitivity of the fitted parameters to the level of background subtraction.

TABLE 2
Einstein Observatory EPHEMERIS FOR ABELL 665 IMAGING DATA

DETECTOR	SEQUENCE NUMBER	DATE	LIVE TIME ^a	FIELD CENTER (1950.0)	
				R.A.	Decl.
IPC	305	1979 Oct 9	6431	8 ^h 26 ^m 18 ^s	66°3'59"
HRI	9971	1980 Sep 23	19762	8 26 18	66 3 59

^a Corrected for detector dead time.

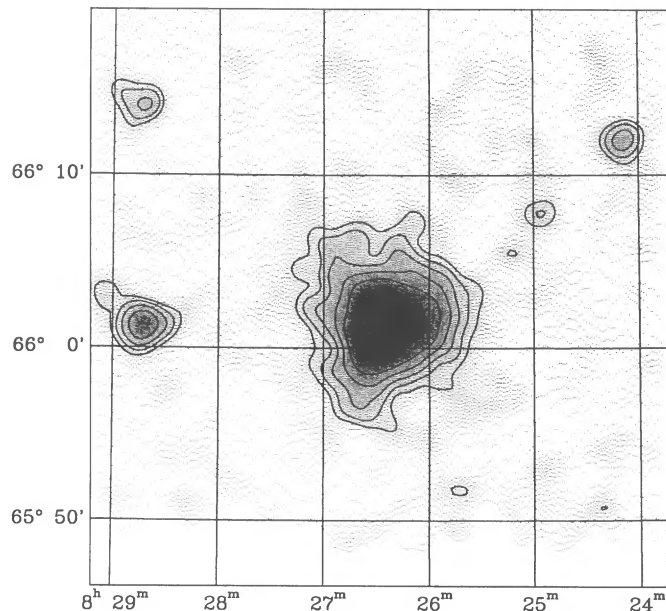


FIG. 2.—Image of the X-ray emission from Abell 665, as observed by the *Einstein* IPC, and generated from the counts by convolution with a Gaussian with $\sigma = 36''$. The lowest contour is drawn at the background level, and higher contours are spaced by equal logarithmic intervals corresponding to multiplication by a factor 1.5. The cluster dominates this image, with three adjacent point sources lying at some distance from the center of the cluster.

The resulting image of Abell 665 is shown in Figure 2, which represents the background-corrected data smoothed by a Gaussian with dispersion $\sigma = 36''$, to decrease fluctuations due to counting statistics. Three point sources appear near the edge of the figure. The two sources to the east have been identified as AGN (Gioia et al. 1990); their IPC spectra are rather hard. The source near the western edge of the map has a soft spectrum (hardness ratio -0.43 , implying an X-ray temperature of about 0.2 keV) and thus is probably a star, although no star appears on the Sky Survey plates at this location. In our spatial analysis we have excluded circular regions of radius $3'$ centered on each of these sources. The possible effect of these contaminating sources on the X-ray spectrum of Abell 665 is examined in Hughes & Tanaka (1991).

The background of the HRI is about an order of magnitude larger than the background of the IPC and is largely intrinsic to the detector. This, coupled with the smaller field of view and lower sensitivity of the HRI relative to the IPC, makes background subtraction more difficult. In contrast to the analysis of the IPC image, it was found that a uniform background gave adequate results, although we note that the background does increase slightly from the center to the edge of the field. The resulting HRI image detected Abell 665 at a confidence level of only about 7σ , and the cluster is not obvious until the HRI image is smoothed by a $\sigma = 20''$ Gaussian. The low counting statistics and the (relatively) high background level of the HRI image render it of little value in fitting the structure of the cluster; the main use of the HRI data is to establish consistency with the IPC image. A particularly important use of the HRI data was in determining the contribution of point sources to the X-ray surface brightness profile: in particular in limiting the contribution of individual galaxies and the dominant central galaxy. No evidence of a brightness spike, such as might arise from a cooling flow, was found in the HRI image.

2.3. The X-Ray Spectra

Observations of the X-ray spectrum of Abell 665 have been made using the Japanese X-ray satellite *Ginga* by Hughes & Tanaka (1991). The analysis of the *Ginga* data is described in detail in that paper, but some details of the observation are necessary here, so that the nature of the errors in the derived temperatures can be understood.

The *Ginga* satellite observed Abell 665 with the Large Area Counters (LAC) on 1988 November 10. Over 2×10^4 s of data were taken during the low-background part of the *Ginga* orbit and were used in the analysis of the spectrum. The higher background part of the orbit was used to scan across Abell 665 to check the position of the cluster, and to check that its emission appeared pointlike to the LAC, so that the data are not contaminated by emission from distant point sources (outside the field of the *Einstein* IPC image of Fig. 2).

For sources as weak as Abell 665, accurate subtraction of the background counts in the LAC is essential if an accurate spectrum is to be obtained. Two procedures were used to remove the background from the LAC data: (1) the background modeling method developed by Hayashida et al. (1989), which involves fitting several parameters that describe the particle-induced background in the LAC and using data from several source-free fields to fit the diffuse X-ray background; and (2) the direct subtraction of data from a source-free field observed during the previous day. The spectra obtained by these different methods proved to be consistent to within their errors up to an energy ~ 13 keV, where the cluster emission is only a small fraction of the background. An upper energy cutoff of 13 keV was therefore used for the LAC spectrum, and the average of the spectra was used in later analysis, with the difference of the spectra providing a measure of the systematic error in the background removal. The lower energy cutoff of the spectrum is 1.5 keV, below which the sensitivity of the LAC declines rapidly.

Further information on the low-energy spectrum of Abell 665 was obtained from the *Einstein* IPC data, which provide useful sensitivity in the energy range 0.2–4 keV. The background level in the IPC is uncertain by about 20%, but a comparison of the flux densities at about 2 keV in the IPC and the *Ginga* LAC found that the relative normalizations of the spectra taken with the two detectors agree to within about 5%. This 5% error reflects the likely systematic error in the flux scale due to uncertainties in the instrumental calibrations, and a 5% systematic error in the X-ray flux scale is adopted in the discussion of the calculation of the Hubble constant in § 3. The spectra of Abell 665 taken with the IPC and LAC are shown in Figure 3, which demonstrates the relative importance of the two data sets in different parts of the overall 0.2–13 keV energy range covered by the composite spectrum.

Figure 3 also shows the high-energy X-ray spectra of Abell 665 that were observed by the *Einstein* Observatory Monitor Proportional Counter (MPC; Gaillardetz et al. 1978). Since the MPC operated in parallel with the imaging instruments, two MPC spectra of Abell 665 are available. The first, taken during the IPC observation, had a live time of 6267 s. The second spectrum, taken during the HRI observation, had a live time of 8274 s. The reduction of the spectral data from the MPC followed the procedure discussed by Arnaud (1991). The consistency of the two independent spectra in both shape and normalization, although they were observed about one year apart, indicates that there are no significant problems in the background subtraction and detector calibration. An external

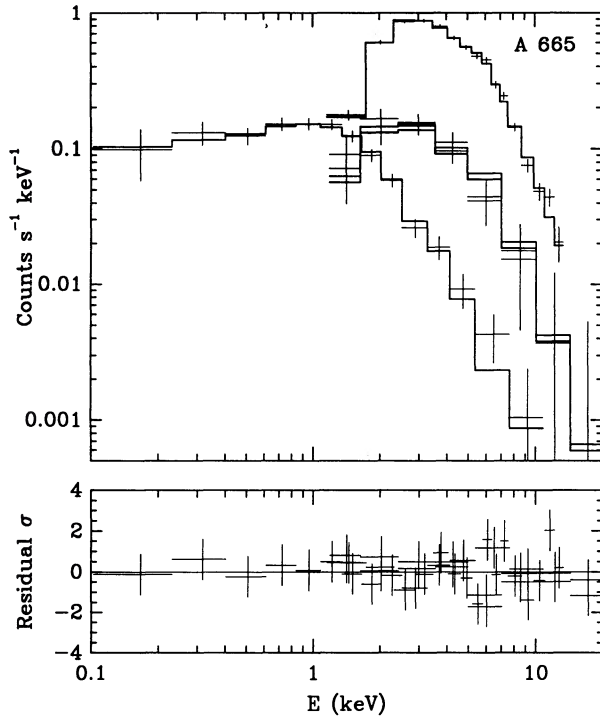


FIG. 3.—X-Ray spectrum for Abell 665. The upper panel shows the data from the *Ginga* LAC (upper set of data points), the *Einstein* MPC (middle two sets of data points, corresponding to the spectra taken during the IPC and HRI observations), and the *Einstein* IPC (lower set of data points). Solid lines indicate the count rates expected from the best-fitting spectrum, which corresponds to an isothermal intracluster medium with $T_e = 8.18$ keV (see § 2.3). The lower panel shows the residuals from the fits: note that the fit is excellent over the full range 0.1–13 keV, and that the spectrum above about 2 keV is largely determined by the *Ginga* data alone.

check of this reduction procedure has been made by comparing spectra of clusters of galaxies observed with both the *Einstein* MPC and the *EXOSAT* ME (Edge et al. 1990)—no systematic bias was found, and the individual measurements of the cluster temperatures are in good agreement. In addition, the normalization of the MPC spectrum is consistent to within about 5% with the normalization of the spectra from the IPC and the *Ginga* LAC.

The background-subtracted data from the three instruments were fitted to redshifted, optically thin, collisional ionization equilibrium models (Raymond & Smith 1977) convolved with the responses of the *Ginga* LAC and the *Einstein* IPC and MPC. Eight free parameters, the temperature and metal abundance of the intracluster medium, the redshift of the cluster, the hydrogen column density along the line of sight, and the normalizations of the four spectra, together with the errors on these parameters, were estimated from this fit. The best-fitting spectrum is superposed on the data in Figure 3. The fit indicates that the temperature of the intracluster medium is $T_e = 8.18^{+0.95}_{-0.81}$ keV (90% error range), or $T_e = 8.18 \pm 0.53$ keV, if the error is expressed as a symmetrical $\pm 1 \sigma$ range. The metal abundance of the gas is $0.46^{+0.16}_{-0.16}$ solar (90% error range), and the hydrogen column density to the cluster is about 4×10^{20} cm $^{-2}$, in agreement with the Galactic value. The redshift fitted from the spectra, 0.15 ± 0.02 , is consistent with the optical spectroscopic redshift. The fit of the data to an isothermal model for the intracluster medium appears anomalously good, $\chi^2 = 21$ with 39 degrees of freedom, because we took account

of the uncertainties in the instrumental calibrations and in the zero levels (i.e., problems with the background subtraction) by adding conservative estimates of these systematic errors in quadrature to the statistical errors in each energy bin in the spectra. In this way we obtain conservative estimates of the errors in the parameters fitted from the spectra. An isothermal fit is found to provide a better description of the spectrum of Abell 665 than any polytropic fit: Hughes & Tanaka (1991) found that the effective polytropic index of the gas in Abell 665 is less than 1.3.

Note that the values that we quote here for the temperature and abundance of the intracluster medium in Abell 665 differ slightly (but not significantly) from the values in Hughes & Tanaka (1991), because of the presence of the *Einstein* MPC data in the present fit.

3. ANALYSIS

3.1. Basic Method

The monochromatic X-ray surface brightness, b_x , and the zero-frequency Sunyaev-Zel'dovich effect, ΔT_{RJ} , of a cluster of galaxies can be expressed as line-of-sight integrals of different functions of the electron concentration (n_e) and the electron temperature (T_e) of the intracluster medium:

$$b_x = \frac{1}{4\pi(1+z)^3} \int n_e^2 \Lambda_e dl, \quad (3.1)$$

and

$$\Delta T_{RJ} = -2T_r \frac{k\sigma_T}{m_e c^2} \int n_e T_e dl. \quad (3.2)$$

In these equations T_r ($=2.74$ K; Kogut et al. 1988) is the temperature of the microwave background radiation, z ($=0.182$) is the redshift of the cluster, $\Lambda_e(E, T_e)$ is the X-ray spectral emissivity of the cluster gas (a function which incorporates the Gaunt factor, the usual exponential energy term, etc.), and the integrals extend over the line of sight (dl). The remaining symbols have their usual meaning. Note that the energy referred to in Λ_e is the emitted photon energy, while the energy referred to in the X-ray surface brightness b_x is the redshifted, observed, photon energy. ΔT_{RJ} is measured in temperature units. Both n_e and T_e are functions of position, r , in the cluster.

It is convenient to express the electron concentration and temperature in terms of a reference electron concentration, n_{e0} , and temperature, T_{e0} (which will be taken to be the central concentration and temperature here, although the values at any fiducial point may be chosen), and dimensionless form factors describing the angular structure of the atmosphere in density, $f_n(\theta, \phi, \zeta)$, and temperature, $f_T(\theta, \phi, \zeta)$, as

$$n_e(r) = n_{e0} f_n(\theta, \phi, \zeta), \quad (3.3)$$

$$T_e(r) = T_{e0} f_T(\theta, \phi, \zeta), \quad (3.4)$$

where a cylindrical angular coordinate system has been used. Here, θ is the angle from a reference line of sight, ζ is an angular measure of distance down the line of sight ($l = \zeta D_A$, where D_A is the angular diameter distance of the cluster), and ϕ is an azimuthal angle about the reference line of sight. Then the energy loss function Λ_e may be written

$$\Lambda_e(E, T_e) = \Lambda_{e0} f_\Lambda(\theta, \phi, \zeta), \quad (3.5)$$

where f_Λ is given by the form factor f_T and the functional dependence of $\Lambda_e(E, T_e)$ on the energy of observation, E , and

T_e . If the intracluster medium is isothermal, then f_T and f_Λ will both equal unity—the temperature and X-ray spectral emissivities are constant over the cluster. If the intracluster medium is polytropic, with $T_e \propto n_e^{\gamma-1}$, then $f_T = f_n^{\gamma-1}$, and f_Λ can also be expressed as a (complicated) function of f_n .

The expressions for the X-ray surface brightness and the Sunyaev-Zel'dovich effect then become

$$b_X(\theta, \phi) = \frac{1}{4\pi(1+z)^3} \Lambda_{e0} n_{e0}^2 D_A \int d\zeta f_n^2 f_\Lambda \quad (3.6)$$

$$\equiv N_X \Theta^{(1)},$$

$$\Delta T_{RJ}(\theta, \phi) = -2T_r \frac{kT_{e0}}{m_e c^2} \sigma_T n_{e0} D_A \int d\zeta f_n f_T \quad (3.7)$$

$$\equiv -N_{RJ} \Theta^{(2)},$$

where the structural information on the cluster is contained in the angles

$$\Theta^{(1)}(\theta, \phi) = \int d\zeta f_n^2 f_\Lambda, \quad (3.8)$$

$$\Theta^{(2)}(\theta, \phi) = \int d\zeta f_n f_T, \quad (3.9)$$

and the normalization of the effects measures the quantities

$$N_X = \frac{D_A}{4\pi(1+z)^3} \Lambda_{e0} n_{e0}^2, \quad (3.10)$$

$$N_{RJ} = 2T_r \frac{kT_{e0}}{m_e c^2} \sigma_T n_{e0} D_A. \quad (3.11)$$

If the normalizations N_X and N_{RJ} can be measured from the X-ray and Sunyaev-Zel'dovich data, and the density and temperature structure of the atmosphere are known (independently, or from images of the X-ray surface brightness or Sunyaev-Zel'dovich effect), then the angular diameter distance of the cluster can be found using

$$D_A = \left(\frac{N_{RJ}^2}{N_X} \right) \left(\frac{m_e c^2}{kT_{e0}} \right)^2 \frac{\Lambda_{e0}}{16\pi T_r^2 \sigma_T^2 (1+z)^3}, \quad (3.12)$$

or, alternatively, the reference density, n_{e0} , may be deduced in a distance-independent manner by eliminating D_A . The Hubble constant can then be found using the value of D_A provided by equation (3.12) and the measured redshift of the cluster.

Since the intrinsic (three-dimensional) density and temperature structures of the cluster (and hence f_n , f_T , and f_Λ) are unknown, it is clear that a wide variety of such structures are likely to be capable of reproducing the (noisy) measurements of the spectrum, b_X , and ΔT_{RJ} shown in Figures 1–3 after allowing for convolution with the responses of the telescopes used. For this reason, some assumptions about the forms of f_n and f_T are crucial to extracting the angular diameter distance of Abell 665, and hence the value of the Hubble constant, from the X-ray and Sunyaev-Zel'dovich effect data. We shall find that relatively simple forms for f_n , f_T , and f_Λ are sufficient to produce good fits to the data. The three assumptions that we make are listed below.

1. It will be assumed that the atmosphere in Abell 665 is isothermal, so that $T_e(r) = T_{e0}$, the central gas temperature. This has the effect of factoring the temperature out of the

problem: $\Lambda_e(T_e)$ becomes a constant, $\Lambda_{e0} \equiv \Lambda_e(T_{e0})$, $f_T = 1$, and $f_\Lambda = 1$.

2.—It will be assumed that the atmosphere is spherical—that $n_e(\mathbf{r})$ may be written as a function of r , the distance from the cluster center, only. Thus $f_n = f_n[(\theta^2 + \zeta^2)^{1/2}]$.

3.—The gas distribution will be assumed to follow a β -model (Cavaliere & Fusco-Femiano 1976, 1978), in which

$$n_e = n_{e0} \left(1 + \frac{r^2}{r_c^2} \right)^{-3\beta/2}, \quad (3.13)$$

so that

$$f_n = \left(1 + \frac{\theta^2 + \zeta^2}{\theta_c^2} \right)^{-3\beta/2}. \quad (3.14)$$

The original intent of this model was that if the distribution of galaxies is described by an analytic approximation to an isothermal sphere (eq. [3.13] with $\beta = 1$), then the distribution of gas follows (eq. [3.13]) where β is a measurement of the relative kinetic energy content of gas and galaxies. For our purposes, equation (3.14) will provide a convenient modeling function, and the values of the angular core radius, $\theta_c = r_c/D_A$, and β will be treated as unknown parameters to be deduced from the X-ray imaging data.

It is clear that if completely general forms for f_n and f_T , perhaps involving substantial small-scale density and temperature structures (“clumping”) are allowed, then it is unlikely that any X-ray or Sunyaev-Zel'dovich effect data can ever provide sufficient constraints on these functions for H_0 to be determined unambiguously. However, provided that the mean values of density and temperature vary slowly over the cluster, and that the amplitude and type of the clumping are also not strong functions of position, strong conclusions on the value of the Hubble constant can still be obtained. The extent to which assumptions (1–3) above can be relaxed, and a result for the value of H_0 can still be achieved, is discussed in § 4.

With these assumptions about the form factors, the angles $\Theta^{(1)}$ and $\Theta^{(2)}$ are independent of ϕ and may be expressed as simple functions of angular offset from the projected cluster center, θ , the core radius, θ_c , and the energy parameter, β . Explicitly,

$$\Theta^{(1)}(\theta) = \sqrt{\pi} \frac{\Gamma(3\beta - \frac{1}{2})}{\Gamma(3\beta)} \theta_c \left(1 + \frac{\theta^2}{\theta_c^2} \right)^{(1/2)-3\beta}, \quad (3.15)$$

$$\Theta^{(2)}(\theta) = \sqrt{\pi} \frac{\Gamma(\frac{3}{2}\beta - \frac{1}{2})}{\Gamma(\frac{3}{2}\beta)} \theta_c \left(1 + \frac{\theta^2}{\theta_c^2} \right)^{(1/2)-(3/2)\beta}, \quad (3.16)$$

which describe the forms of the X-ray and Sunyaev-Zel'dovich surface brightnesses of the cluster. For comparison with the observational data these functions must be convolved with the responses of the telescopes.

The form of equation (3.12) indicates the relative importance of the various observables in determining the accuracy of the distance estimate. It is clear, for example, that since D_A depends on N_{RJ} and T_{e0} as the square (Λ_e is a fairly slowly varying function of T_e), the accuracy with which these parameters can be estimated is likely to limit the accuracy with which D_A is found. Accordingly, it is critical that the errors in these two quantities be well understood: this is a particular concern for N_{RJ} , where large systematic errors have led to strong disagreements between independent observations of the same cluster.

3.2. Fits to the X-Ray Images and the Sunyaev-Zel'dovich Effect Data

The values of the normalizations N_X and N_{RJ} (and of the relative normalization N_{RJ}/N_X , which appears in eq. [3.12]) depend on the forms of $\Theta^{(1)}$ and $\Theta^{(2)}$, and hence on the parameters β and θ_C which characterize the shape of the cluster atmosphere. The range of models permitted by the data can be found by fitting the shapes of the X-ray emission and Sunyaev-Zel'dovich effect to the observed structural data. The normalizations of these fits are just the quantities N_X and N_{RJ} required to calculate D_A , and for consistency the same set of parameters (β , θ_C) must provide adequate fits to both the X-ray and Sunyaev-Zel'dovich effect data.

In most analyses to date, X-ray imaging data on clusters of galaxies have been converted to radial surface brightness profiles for model fitting after the center of the cluster has been decided (see, e.g., Jones et al. 1979; Abramopoulos & Ku 1983). A superior procedure is to fit the two-dimensional distribution of counts in the IPC and HRI images directly to model surface brightness distributions. This allows us to fit the background level over large regions of the image, to determine the cluster center while simultaneously fitting the parameters of the isothermal β model, and to search for (and fit) multiple spatial components in the X-ray surface brightness.

X-ray images tend to be sparsely filled; many image pixels have no counts, and it is rare for extended sources to yield even ten counts in any single pixel. This is certainly the case for the Abell 665 (Fig. 2). In such situations it is not possible to employ the usual χ^2 statistic as the figure-of-merit function. The χ^2 statistic requires that measurement errors be Gaussian-distributed; errors obtained by counting experiments are distributed as a Poisson distribution. Only when the number of counts is large enough (> 10) does the Poisson distribution tend toward a Gaussian distribution. This led us to use a maximum-likelihood statistical estimator explicitly derived for the case where measurement errors are Poisson-distributed (this is a robust estimator of the M-estimator category; Press et al. 1986). We used this estimator to determine best-fit values for β , θ_C , and N_X in equations (3.6) and (3.15) and to generate confidence intervals for those parameters.

Unlike the χ^2 statistic, our maximum-likelihood estimator does not yield a goodness-of-fit criterion. Two ancillary tests were developed for this. First a normalized cumulative distribution of all the fitted counts in the actual image was compared to the cumulative distribution of the predicted counts in the model image, and the maximum unsigned deviation between the two distributions was obtained. The Kolmogorov-Smirnov test was applied to check that the distributions are similar. The second goodness-of-fit criterion involved a χ^2 test on the data binned radially about the derived center and fitted to a one-dimensional surface brightness model (with parameters from the two-dimensional fits). The χ^2 value was examined for its significance level. Our best-fit single-component isothermal β model for Abell 665 was found to be acceptable under both methods. Thus there is no evidence in the X-ray image of Abell 665 for any substructure in the cluster as strong as the substructure in the galaxy distribution described by Geller & Beers (1982). Some improvement in the goodness of fit is achieved if two isothermal β -models are used to describe the X-ray structure of Abell 665: this is explored further in § 4.2, but in the remainder of this section the single-component model will be used since it provides an adequate description of the X-ray structure of Abell 665.

The parameters resulting from the fit to any one (β , θ_C) model are the location of the center of the gas distribution of the cluster, the normalization (N_X), and a statistic representing the quality of fit. As explained earlier, the IPC data provide a better representation of the overall structure of the cluster atmosphere than the HRI data and provide the best estimates for β and θ_C . The HRI data provide a check that this model atmosphere is consistent with the central part of the gas distribution as well as the outer parts (i.e., that there is no X-ray "spike" produced by, e.g., a cooling flow of gas into the central galaxy).

On the basis of the IPC fits, the center of the Abell 665 atmosphere is ($08^{\text{h}}26^{\text{m}}25^{\text{s}}$, $66^{\circ}01'21''$, 1950.0), which is consistent with the fitted center of the HRI image, at ($08^{\text{h}}26^{\text{m}}24^{\text{s}}$, $66^{\circ}00'50''$, 1950.0) given the accuracy with which the centroid can be located (about $\pm 20''$ in each coordinate). The cD galaxy in Abell 665 lies at ($08^{\text{h}}26^{\text{m}}24^{\text{s}}.63 \pm 0^{\text{s}}.14$, $66^{\circ}00'35''.2 \pm 0''.4$, 1950.0), as measured from the Palomar Sky Survey. This appears to be somewhat south of the center of the gas distribution, but the X-ray center is too imprecisely known for this to be clear.

However, the cluster center, as defined either by the X-ray center or the location of the cD galaxy (which lies close to the location of the peak galaxy density; Geller & Beers 1982), lies significantly to the south of the cataloged center position for Abell 665 (as given in 1950.0 coordinates by Sastry & Rood 1971; $08^{\text{h}}26^{\text{m}}12^{\text{s}}$, $66^{\circ}04'00''$). It is interesting to note that the Sunyaev-Zel'dovich measurements of Abell 665, made ignorant of the offset between the gas center and the Abell center of the cluster, independently show that such an offset exists—this provides a useful confirmation of the reality of the Sunyaev-Zel'dovich effect in Abell 665.

Confidence level contours for fits of the form of equations (3.6) and (3.15) to the IPC data are shown in Figure 4. It can be seen that the best-fit model has $\beta = 0.66$ and $\theta_C = 1.6$. A value of $\beta \approx 0.7$ is normal for a rich X-ray cluster (Forman & Jones 1982)—for example, the Coma cluster can be well fitted with $\beta = 0.68$ (Hughes et al. 1988). Similarly, the X-ray core radius θ_C of the Coma cluster is $10'$, which would imply a core radius ≈ 1.6 if it lay at the redshift of Abell 665. Thus in both β and core radius, Abell 665 is similar to the Coma cluster. Note, that, formally, $\beta = 0.66$ is not physically realistic since it corresponds to an atmosphere with infinite gas mass. However, the divergence at large radius is slow, and an outer cutoff at large radius will not have a significant effect on the X-ray or the SZ effect profile of Abell 665. In what follows, we shall use all values of β and θ_C on the model plane of Figure 4 without further comment.

The details of the fit to the X-ray structure depend critically on the calibrations of the X-ray data, especially on the background subtraction. An underestimate of the background count level in the image would bias the fitted parameters to a larger, more diffuse atmosphere (larger θ_C and smaller β): an overestimated background would have the opposite effect. The likely extent of this systematic error on the fits for β , θ_C , and N_X has been estimated by repeating the fits with backgrounds 20% higher and lower than the nominal value. It was found that, provided that not too large a region on the X-ray image was fitted, variations of less than 1% in N_X and much less than the random errors in β and θ_C are produced.

The Sunyaev-Zel'dovich data can also be fitted to find the best values of β and θ_C , as well as N_{RJ} . However, since these data are restricted to a single NS cut through Abell 665, the

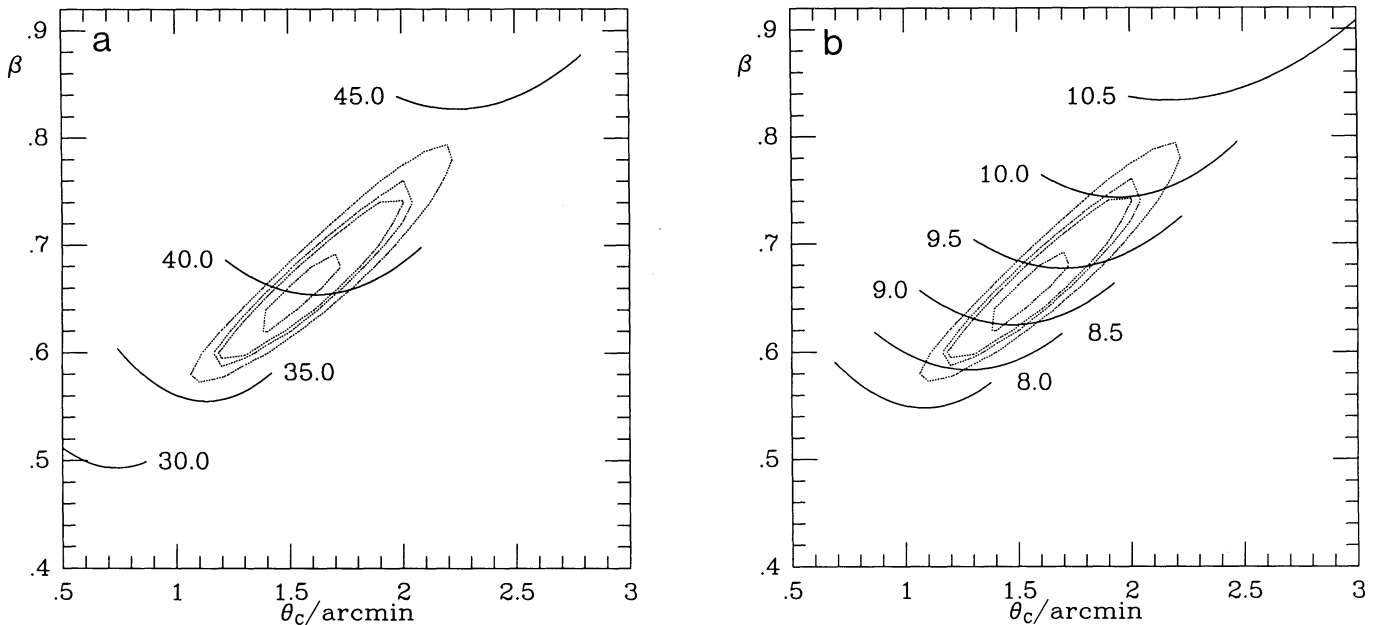


FIG. 4.—Confidence level contours for fits of isothermal β -models to the IPC image of Abell 665, with superposed contours of the value of H_0 (in $\text{km s}^{-1} \text{Mpc}^{-1}$) derived from the X-ray and Sunyaev-Zel'dovich effect data. The best fit lies at $\beta = 0.66$, $\theta_c = 1'.6$, and corresponds to $H_0 = 40 \text{ km s}^{-1} \text{Mpc}^{-1}$. (a) Fitted values of $H_0/\text{km s}^{-1} \text{Mpc}^{-1}$ superposed on contours corresponding to confidence levels of 50%, 90%, 95%, and 99%. (b) Errors on the fitted values of $H_0/\text{km s}^{-1} \text{Mpc}^{-1}$, superposed on confidence level contours as in (a). These errors were calculated taking account of only the random errors in the X-ray and microwave background data.

position of the center of the gas distribution perpendicular to the cut must be taken from the X-ray fits. When this is done the center of the atmosphere in declination is fitted to be $66^\circ 02' 20'' \pm 25''$, 1.0 ± 0.5 north of the fitted X-ray center. If this offset is real, then it implies that the peak gas density (which is essentially located by the X-ray fit) lies away from the geometric center of the overall gas distribution. The change in χ^2 as the center of the SZ fit is moved from the X-ray position is 6.9, corresponding to a significant improvement in the fit. If this difference in the fitted X-ray and SZ centers is real, then the assumption of a spherically symmetric (or even ellipsoidally symmetric) gas distribution is wrong (see § 4.1), and hence the simple forms assumed for f_n and f_T in § 3.1 are not entirely accurate. However, the change in the normalization of the Sunyaev-Zel'dovich data that is produced by taking the X-ray center as the center of the cluster, rather than using the Sunyaev-Zel'dovich data alone, is smaller than the random fitting error on the normalization, so that the uncertainty in the registration of the X-ray and SZ data probably has little effect on the result for H_0 , except to the extent that it indicates difficulties with such a simple model for the cluster gas.

Whether the location of the center of the gas distribution is left free, or fixed at the X-ray centroid, the Sunyaev-Zel'dovich data are neither sufficiently extensive nor sufficiently precise to allow β and θ_c to be estimated together from the fits: for essentially any value of $\beta > 0.4$, an adequate fit can be found for some value of θ_c —in particular, the parameters deduced from the X-ray image ($\beta = 0.66$, $\theta_c = 1'.60$) are acceptable, although a larger θ_c is a marginally better fit (χ^2 decreases by 1.7 as θ_c is increased from 1.60 to the best fit, at $\theta_c = 3'.1$).

Using the X-ray-fitted model, the normalization of the Sunyaev-Zel'dovich data is

$$N_{\text{RJ}} = 181 \pm 16 \mu\text{K arcmin}^{-1}, \quad (3.17)$$

and the value of $\chi^2 = 11.0$ with 6 degrees of freedom. This is a

relatively poor fit (the probability of obtaining a larger value of χ^2 by chance is 9%). More than half the contribution to χ^2 in this fit comes from a single point in the scan (the point at $66^\circ 06'$), which, like the point at $66^\circ 08'$, is contaminated by the presence of Moffet & Birkinshaw's (1989) source 14. There is reason to suspect that the source corrections at these points are subject to an additional systematic error: the variation with time of their apparent Sunyaev-Zel'dovich effect suggests that source 14 is variable (Birkinshaw et al. 1991). If an attempt is made to take account of this variability, which has different effects at $66^\circ 06'$ and $66^\circ 08'$ because the mean dates of observation at these points are different, then the contribution to χ^2 from the point at $66^\circ 06'$ halves, and the fit becomes entirely acceptable. Almost no change in the fitted value of N_{RJ} is obtained through this change (because the value of N_{RJ} depends principally on the values measured closer to the center of the cluster), and removing the point at $66^\circ 06'$ from the fit entirely also has only a small effect. A large systematic error because of the variability of source 14 may also explain the 1.0 ± 0.5 offset of the X-ray and Sunyaev-Zel'dovich effect centroids of the cluster.

If the possibility of systematic errors (as shown in Fig. 1) is incorporated into the fits in a general way, then it is clear that significant variations in the fitted normalization N_{RJ} , and the best-fit values of β and θ_c can result if the systematic offsets are correlated across the scan. Varying a single scan point within its systematic errors has a much smaller effect (for example, varying the Sunyaev-Zel'dovich signal at the peak causes a change in N_{RJ} less than the random error). For this reason, the most serious of the systematic uncertainties is the uncertainty in the zero level of the scan. If the model suggested by the X-ray fit ($\beta = 0.66$, $\theta_c = 1'.60$) is adopted, then decreasing the zero level of the Sunyaev-Zel'dovich effect scan from its nominal value (of $0 \mu\text{K}$) to the lower limit of its range ($-41 \mu\text{K}$) causes a steady improvement in the χ^2 of the fit, from 11.0

to 9.0, indicating a slight preference for a reduced zero level (further reductions in the zero level reverse this trend, increasing χ^2 again: a zero level reduced below $-100 \mu\text{K}$, as would be needed to decrease the angular diameter distance by a factor of 2, can be ruled out on statistical grounds if the χ^2 curve as a function of zero level is used to estimate the zero level). The variation in the fitted value of N_{RJ} caused by the reduction of the zero level from 0 to $-41 \mu\text{K}$ is from 181 to 159 $\mu\text{K arcmin}^{-1}$. This potential 12% systematic error in N_{RJ} dominates the systematic error sum in the Sunyaev-Zel'dovich effect normalization and may have a particularly pernicious effect on the result for H_0 since the offset is *one-sided*.

Finally, it should be recalled that there is a scale error of about $\pm 6\%$ in N_{RJ} because of the uncertainty in the efficiency of the 40 m telescope.

The results of all these fits are, therefore, that the X-ray and Sunyaev-Zel'dovich data are each consistent with isothermal models of the intracluster medium in Abell 665 with a density structure of the form in equation (3.13) and $\beta \approx 0.66$, $\theta_c \approx 1'.6$ centered on (08^h26^m25^s, 66°01'20", 1950.0). The random component of the errors in the X-ray normalization near this best fit is about 3%, and a further systematic component in the error of about 5% is implied by uncertainties in the background level, the overall flux calibration, and the energy response of the *Einstein* IPC. The Sunyaev-Zel'dovich effect normalization, N_{RJ} , shows random errors $\approx 9\%$ near the best fit, with a systematic offset of up to 12% from the zero level error (which dominates and is asymmetrical about a value of N_{RJ} that is 6% smaller than is given in 3.17). The value of N_{RJ} is also subject to a multiplicative uncertainty of about 6% from the uncertainty in the efficiency of the 40 m telescope. Other residual systematic errors are negligible.

3.3. The Value of the Hubble Constant

The results for N_{RJ} , N_x , and T_e from the SZ data, the *Einstein* imaging data, and the *Einstein* and *Ginga* spectral data can now be used in equation (3.12) to deduce the value of the Hubble constant on the assumption that a simple, unclumped, isothermal model of the cluster atmosphere is adequate. The result, assuming that the systematic errors are small, is shown in Figure 4a. It can be seen that near the best-fitting model (represented by the confidence contours for fits to the X-ray image) the value of H_0 is only a weak function of β and θ_c and lies near $40 \text{ km s}^{-1} \text{ Mpc}^{-1}$. Using only the random errors in T_e , N_{RJ} , and N_x , the errors in H_0 are shown in Figure 4b. Apparently the value of the Hubble constant is well determined by this single cluster and is in better agreement with a large universe than a small universe: the overall result is

$$H_0 = 40 \pm 9 \text{ km s}^{-1} \text{ Mpc}^{-1}, \quad (3.18)$$

where the error includes a component from the uncertain metallicity of the cluster gas (§ 2.3) as well as from the random errors in T_e , N_x , and N_{RJ} .

We must now assess the possible changes in H_0 produced by the systematic errors in the data. The more fundamental errors caused by the uncertain physical models for the cluster atmosphere are addressed in § 4. The components of the systematic error that relate to the data are caused by

1.—Residual systematic errors in N_x , principally from the uncertain background in the X-ray images. According to the estimates in §§ 2.2 and 2.3, this error is less than 5%, and so a range of -2 to $+2 \text{ km s}^{-1} \text{ Mpc}^{-1}$ about the best-fit value of H_0 is assessed for this error;

2.—Residual systematic errors in T_e , principally from the uncertain background in the *Ginga* spectrometer. The maximum range of systematic error in the temperature is comparable with the random error, or about 6%. This corresponds to about a 12% variation in the value of H_0 , which leads to a systematic offset range of -5 to $+5 \text{ km s}^{-1} \text{ Mpc}^{-1}$;

3.—Residual systematic errors in N_{RJ} . According to the discussion above, these errors are dominated by the uncertainty in the gain of the 40 m telescope (a 6% effect), and by the possibility of variations in the absolute zero level of the microwave background data (which causes an asymmetrical variation in N_{RJ} , from -12% to 0%). As can be seen from equation (3.12), the weight of N_{RJ} in the estimate for H_0 is similar to the weight of T_e : the larger possible systematic errors in N_{RJ} therefore make this the most important contributor to systematic errors in H_0 ; producing a systematic offset range of 0 to $+10 \text{ km s}^{-1} \text{ Mpc}^{-1}$, and a systematic scale error of $\pm 12\%$ in H_0 ; and

4.—Some account should also be taken at this stage of the model dependence of the estimate for H_0 . From Figure 4a, it can be seen that the 90% error ellipse for fitting the X-ray image encompasses values of H_0 varying by up to $\pm 3 \text{ km s}^{-1} \text{ Mpc}^{-1}$.

If these systematic errors are combined in quadrature, they correspond to an error of $\pm 8 \text{ km s}^{-1} \text{ Mpc}^{-1}$ about a center that is $0\text{--}10 \text{ km s}^{-1} \text{ Mpc}^{-1}$ larger than the best-fit value for H_0 . If the total systematic error is now combined in quadrature with the statistical error on the estimate for the Hubble constant, the overall result becomes

$$H_0 = (40 \text{ to } 50) \pm 12 \text{ km s}^{-1} \text{ Mpc}^{-1}. \quad (3.19)$$

A more conservative approach is to assume a worst case combination of the systematic errors by adding them directly. The result for the Hubble constant then becomes

$$H_0 = (26 \pm 8) \text{ to } (65 \pm 10) \text{ km s}^{-1} \text{ Mpc}^{-1}. \quad (3.20)$$

In either case, it appears that the long ($H_0 \approx 50 \text{ km s}^{-1} \text{ Mpc}^{-1}$) distance scale for the universe is supported over the short ($H_0 \approx 100 \text{ km s}^{-1} \text{ Mpc}^{-1}$) distance scale.

From this discussion it can be seen that the greatest improvement in the accuracy of equation (3.19) can be obtained by achieving tighter limits on possible zero level offsets in the Sunyaev-Zel'dovich data and by improving the quality of the X-ray spectrum of Abell 665. The former improvement requires more extensive observations away from the center of the gas distribution in Abell 665 and further observations of the radio source environment of the cluster: both programs are presently feasible. Further improvements in the X-ray spectrum of the cluster require larger, and higher angular resolution, X-ray telescopes capable of measuring moderately hard spectra. Such developments are possible, but new data of this type are not likely to appear in the near future. A more profitable approach to improving the Hubble constant estimate is, therefore, to apply this method to other clusters of galaxies for which high-quality X-ray and Sunyaev-Zel'dovich data exist.

We may compare the precision of equation (3.19) with the precision of other measurements of the Hubble constant. At redshift $z \lesssim 0.003$, the peculiar motions of galaxies dominate over the Hubble flow, and no reliable measurement of H_0 from a single object will be possible. There are few accepted distance tracers that work at redshifts greater than 0.003: the three principal methods that have been used involve supernovae as

standard candles (van den Bergh 1988), the (infrared) Tully-Fisher relation (Aaronson et al. 1986); and the D_n/σ correlation (Dressler et al. 1987). The dispersion in supernova peak magnitudes exceeds 0.7 mag for any of the supernova types used for distance measurements, and thus no single supernova measurement can give a distance with a precision $\gtrsim 30\%$. This is somewhat greater than the random error on H_0 (in eq. [3.18]), but an improvement on the overall range given in equation (3.19) or (3.20). The infrared Tully-Fisher relation, for any one galaxy, has a scatter of about 0.3 or 0.4 mag, corresponding to about a 15% distance error per object, similar to the scatter of the D_n/σ relation. Clearly both these methods are currently superior to the Sunyaev-Zel'dovich/X-ray method. The gain in using the Sunyaev-Zel'dovich effect is that of circumventing entirely the local distance indicators and calibrators for the distance scales (necessary, and a source of systematic error, in all these three methods). The defect in using this method is that the accuracy is presently low, because of the possibility of residual systematic errors, and because of our incomplete understanding of the physical properties of the cluster of gal-axes being used as a distance tracer (§ 4).

4. DISCUSSION

The result (eq. [3.19]) for H_0 , deduced from the X-ray and Sunyaev-Zel'dovich data, is based on the simplest model for the atmosphere of Abell 665. The cluster gas was assumed to be spherically distributed, isothermal, unclumped, and accurately described by a simple β -model (eq. [3.13]). The X-ray and Sunyaev-Zel'dovich data were assumed to be uncontaminated by other effects. In this section we consider the effects of relaxing these assumptions, and attempt to evaluate the potential usefulness of this approach to the determination of H_0 .

4.1. An Aspherical Cluster Atmosphere

Simple limits to the effects of asphericity on the estimate of the Hubble constant can be deduced by supposing that the atmosphere is prolate or oblate, rather than spheroidal, with the unique axis oriented along the line of sight. This is, in a sense, the most extreme variation of the geometry of the original spherical model: if the unique axis is oriented in any other direction, some change in the shape of the X-ray isophotes should be measurable. However, if the unique axis lies along the line of sight, then the apparent X-ray surface brightness (or Sunyaev-Zel'dovich effect; or galaxy distribution) will have a circular symmetry, and it will be difficult to determine that such a distortion of the cluster exists.

If the orientation of the unique axis is along the line of sight, with the core radius of the gas density distribution in this z -direction larger by a factor Z than the core radii in the other two directions, the density form factor will follow

$$f_n = \left[1 + \frac{x^2 + y^2 + (z^2/Z^2)}{r_c^2} \right]^{-3\beta/2}, \quad (4.1)$$

$$= \left[1 + \frac{\theta^2 + (\zeta^2/Z^2)}{\theta_c^2} \right]^{-3\beta/2} \quad (4.2)$$

rather than equation (3.14); $Z > 1$ corresponds to a prolate gas distribution, while $Z < 1$ corresponds to an oblate distribution. With this modification, the integrals in equations (3.8) and (3.9) scale by a factor Z , but are otherwise unchanged. Forms (3.6) and (3.7) for b_x and ΔT_{RJ} can be retained, as can forms (3.15) and (3.16) for $\Theta^{(1)}$ and $\Theta^{(2)}$, but the expressions for

the X-ray and Sunyaev-Zel'dovich effect normalizations become

$$N_x = \frac{D_A}{4\pi(1+z)^3} \Lambda_{e0} n_{e0}^2 Z, \quad (4.3)$$

$$N_{RJ} = 2T_r \frac{kT_{e0}}{m_e c^2} \sigma_T n_{e0} D_A Z, \quad (4.4)$$

where it can be seen that a prolate distribution tends to produce a larger central surface brightness in both effects.

Equation (3.26) for the angular diameter distance of the cluster is then also modified, and becomes

$$D_A = \left(\frac{N_{RJ}^2}{N_x} \right) \left(\frac{m_e c^2}{kT_{e0}} \right)^2 \frac{\Lambda_{e0}}{16\pi T_r^2 \sigma_T^2 (1+z)^3} \frac{1}{Z}, \quad (4.5)$$

so that the value of D_A calculated assuming $Z = 1$ (as was used in § 3) will differ from the true angular diameter distance of the cluster by a factor

$$\frac{D_A(\text{true})}{D_A(\text{estimated})} = \frac{1}{Z}. \quad (4.6)$$

If the cluster is highly prolate, then $Z \gg 1$, and the true angular diameter distance will be much smaller than the distance deduced on the basis of equation (3.26). Thus if the cluster is prolate, with the unique axis along the line of sight, the value of the Hubble constant estimated in § 3 will be an underestimate.

According to Carter & Metcalfe (1980), the distribution of galaxies in a cluster of galaxies is typically quite elliptical—the median ellipticity that they found was E5. The X-ray isophotes of clusters are also often elliptical with ellipticities up to about E5 being common (e.g., for the Coma cluster, Hughes et al. 1988). Clearly the appreciable nonsphericity of the typical cluster can contribute a considerable uncertainty to the calculated value of H_0 : if clusters are often E5 in shape, then for any given cluster, $0.5 \lesssim Z \lesssim 2$. Thus the likely error in the derived value of H_0 from the intrinsic variations in the shapes of clusters of galaxies will be a factor ≈ 2 .

Some protection against this effect could be gained by applying the method to a sample of clusters of galaxies, but it is important that this sample be selected on the basis of *integrated* X-ray flux, rather than central X-ray surface brightness or strength of the Sunyaev-Zel'dovich effect. A sample selected from the central X-ray surface brightness or Sunyaev-Zel'dovich effect would be naturally biased toward prolate objects, since N_x and N_{RJ} are proportional to Z .

In summary, if Abell 665 is prolate, with the unique (long) axis lying close to the line of sight, then the value of the Hubble constant found in § 3 may be an underestimate by a factor of up to 2 merely because of this asphericity. If Abell 665 is oblate, then the value of the Hubble constant may be overestimated by a factor of up to 2.

4.2. Large-Scale Substructure in the Cluster Atmosphere

Abell 665, like many other clusters of galaxies, is known to exhibit significant substructure in its galaxy distribution (Geller & Beers 1982). Two prominent peaks in the galaxy distribution can be seen in Geller & Beers' contour map of Abell 665: the strongest peak is centered near the cD galaxy, and a second peak lies about $10'$ to the northwest. However, the X-ray image of Abell 665 does not show any similar structure. The centroid of the X-ray emission corresponds closely to

the southern peak in the galaxy distribution, and there is no detectable X-ray emission associated with the other group of galaxies. Although it appears that the northwestern peak of the galaxy counts is not associated with the X-ray-emitting medium in Abell 665, radial velocity measurements of galaxies in both parts of the cluster would be helpful in interpreting the structure in terms of a double cluster, or two clusters which happen to lie near the line of sight.

Although the X-ray structure of the cluster is not sub-clustered like the galaxies, on angular scales $\approx 10'$, inspection of Figure 2 reveals significant deviations from circular symmetry in the central isophotes of the X-ray emission. In order to assess the significance of this structure, we carried out fits to the IPC image with multiple β -models using our software for fitting two-dimensional image data. Because of the small angular size of the cluster compared to the spatial resolution of the IPC, and the limited counting statistics in the image, we restricted ourselves to two components, and in addition we required that the two components have the same β and θ_C values. The positions and normalizations of each component, and the overall values of β and θ_C , were free parameters of the fit.

The fit to the surface brightness of the X-ray image of Abell 665 is improved significantly by the addition of a second β -model component (the three new parameters that are introduced improve the fit at better than the 3σ confidence level). The new best-fit β model has $\beta = 0.62$ and $\theta_C = 1.20$, with the brightest component remaining near the best-fit position found from the single-component fit (§ 3.2), and the fainter component centered 1.2 north and 2.4 west of this position. The intensity of this subsidiary, offset, component is only 16% of the intensity of the dominant, central, component.

If it is assumed, conservatively, that the Sunyaev-Zel'dovich effect that is observed arises only from the brighter X-ray component, in this fit, then the value of H_0 that is calculated is lower than the central value (eq. [3.19]) because of the smaller values of θ_C and N_X that are fitted (see Fig. 4 and eq. [3.12]). However, the total change in H_0 is only $8 \text{ km s}^{-1} \text{ Mpc}^{-1}$, of which about $3 \text{ km s}^{-1} \text{ Mpc}^{-1}$ is contributed by the change in θ_C and $5 \text{ km s}^{-1} \text{ Mpc}^{-1}$ by the reduction in N_X . This is less than the estimate of the error in the Hubble constant in equation (3.19).

The observed substructure in the X-ray image of Abell 665, although statistically significant, appears on the same angular scale as the resolution of the *Einstein* IPC. More detailed investigation into the X-ray structure of the cluster awaits deeper images, such as might be made with *ROSAT*, or high spatial resolution at high sensitivity, as should be produced by *AXAF*.

4.3. A Clumpy Cluster Atmosphere

A major simplification that is implicit in the choice of equation (3.13) for the distribution of density in the cluster is that the density variations on scales unresolved by the images are small (i.e., that the medium is not clumpy). Strong clumping on small scales has the effect of increasing the X-ray emissivity of the gas relative to the strength of the Sunyaev-Zel'dovich effect, and such clumping could not be detected directly in the data available to us. We characterize such small-scale clumping by a parameter

$$C = \frac{\langle n_e^2 \rangle}{\langle n_e \rangle^2}, \quad (4.7)$$

where the averages are taken over regions small compared with the scale of the X-ray telescope's resolution. Variations in C across the cluster can be expressed in terms of a fiducial clumping factor, C_0 , and a form factor, f_C , in the same way that the smooth density variation is characterized by n_{e0} and f_n , but it is unlikely that such variations will be amenable to observational test. The uncertainty caused by small-scale clumping will therefore be described by a single value of the clumping parameter, C_0 , assumed to be a constant over the cluster. The expressions for N_{RJ} , $\Theta^{(1)}$, and $\Theta^{(2)}$ are unchanged by the introduction of this parameter, while the X-ray normalization is now given by

$$N_X = \frac{D_A}{4\pi(1+z)^3} \Lambda_{e0} n_{e0}^2 C_0. \quad (4.8)$$

Then, following the arguments leading to equation (3.12), the value of the true angular diameter distance differs from the value of D_A deduced by assuming that the medium is unclumped ($C_0 = 1$) by a factor

$$\frac{D_A(\text{true})}{D_A(\text{estimated})} = C_0, \quad (4.9)$$

so that if $C_0 > 1$, and the intracluster medium is significantly clumped, the true angular diameter distance is larger than that deduced by assuming $C_0 = 1$, and the true value of the Hubble constant is smaller than was deduced in § 3. If the typical clumping in a cluster atmosphere is not isothermal, then the value of C_0 in equation (4.8) takes a different meaning, becoming now

$$C_0 = \frac{\langle n_e^2 \Lambda(T_e) \rangle}{\langle n_e \rangle^2 \langle \Lambda(T_e) \rangle}, \quad (4.10)$$

since the variations in n_e and T_e may be correlated.

It is difficult to set useful limits to C_0 on the basis of the observations, since C_0 has been defined in terms of structures on scales less than the experimental resolution. If the inhomogeneities are nonisothermal (e.g., isobaric), a detailed study of the X-ray spectrum of a cluster might set some limits to C_0 for some assumed $n_e(T_e)$ in the perturbations, but the conclusions that might be reached are likely to be strongly model-dependent (since, for example, fluctuations of a given fractional amplitude in the high-density core of the cluster will produce larger changes in the X-ray spectrum than will similar fluctuations in the outer part of the cluster) and rather weak for a cluster of such low signal strength as Abell 665.

A theoretical calculation of the clumping of the intracluster medium would be difficult, since it must take into account the many processes tending to cause clumping (gas injection from the galaxies, energy input from the galaxy motions, etc.), as well as the dissipational processes that tend to erase clumps (thermal conduction, mixing by galaxy motions, gas-dynamical processes, etc.). No useful calculation of this type has been performed. However, it is clear that if the intracluster medium is exceedingly clumpy, with a very large value of C_0 , it tends to radiate energy more efficiently than an unclumped medium. This would drive a strong cooling flow and hence cause the typical X-ray brightness spike in the center of the cluster that is often used as an indication of a cooling flow's presence. Thus the absence of a clear spike in the HRI image of Abell 665, which implies the absence of a strong cooling flow in the cluster, can be used to set a weak limit to the value of C_0 , $C_0 \lesssim 3$, and hence a weak limit on the overestimation of the

value of the Hubble constant caused by clumping (the inverse argument, that if $H_0 \sim 50 \text{ km s}^{-1} \text{ Mpc}^{-1}$, then C_0 is not large, is of interest in the study of cluster atmospheres).

Clumping is not a quantity that can be averaged out from cluster to cluster: all cluster atmospheres will be clumpy to some degree, and hence all clusters will tend to have values of $C_0 > 1$. This implies that the value of the Hubble constant deduced by applying this method to a large sample of clusters can never be more than an upper limit to the value of the true Hubble constant, although if the typical clumping parameter of a cluster is close to one, the error involved may be small.

In summary, although tighter constraints on C_0 might be obtained by making a more detailed analysis of the thermal structure of the cluster atmosphere, and of the survival of temperature fluctuations within it, at present we can only estimate that the effects of clumping cause a decrease of less than a factor ~ 3 in the value of the Hubble constant below our best estimate (eq. [3.19]).

4.4. Thermal Structure

The calculation so far has assumed that Abell 665 has an isothermal atmosphere, so that $f_T = 1$. This assumption is supported by the X-ray spectrum of the cluster (Hughes & Tanaka 1991), which is fitted better by an isothermal model than by any polytropic model, but the X-ray data are most sensitive to the gas properties in the densest part of the cluster since the X-ray emissivity is proportional to n_e^2 . For an isothermal gas distributed according to equation (3.12) with $\beta = 0.66$, 80% of the central X-ray surface brightness comes from gas within one core radius of the cluster center. The gas responsible for the Sunyaev-Zel'dovich effect is more widely distributed—on this same model, only 40% of the central Sunyaev-Zel'dovich effect comes from gas within one core radius of the cluster center, and it requires gas out to four core radii to contribute 80% of this signal. On average, therefore, the gas responsible for the Sunyaev-Zel'dovich effect is several times more distant from the cluster center than the gas responsible for the X-ray emission.

Thus if the cluster core is surrounded by a hot, low-density medium, then the X-ray emissivity of that gas can be low while the line-of-sight integral of the pressure of the gas (and hence its contribution to the Sunyaev-Zel'dovich effect) remains large. The fitted value of N_{RJ} can then contain a contribution from gas that is not represented in the X-ray surface brightness. If only a fraction v_{RJ} of the fitted value of N_{RJ} is associated with the X-ray-emitting gas, then the angular diameter distance calculated assuming that $v_{\text{RJ}} = 1$ will differ from the true angular diameter distance by a factor

$$\frac{D_A(\text{true})}{D_A(\text{estimated})} = v_{\text{RJ}}^2. \quad (4.11)$$

Very widespread halos of gas are removed by the background subtraction in the X-ray images, and by the beam-switching in the radio observations, so that some discrimination against values of v_{RJ} far from unity is implicit in the observational method. The similarity of the fitted parameters β and θ_c based on the X-ray and Sunyaev-Zel'dovich effect data also suggests that $v_{\text{RJ}} \sim 1$: it is unlikely that $v_{\text{RJ}} < 0.7$, so that the Hubble constant is unlikely to be underestimated by a factor greater than 2. Further estimates of the value of v_{RJ} could be based on the observation that not all clusters can have large, low-density, high-temperature halos, or the diffuse X-ray back-

ground would be overproduced (but this is only an average constraint, and may not apply to a single cluster). The absence of a cool halo of gas around the cluster is assured by absence of a "rim" of radio emission from the thermal bremsstrahlung of an (unstable) shell of cool gas.

An alternative type of thermal structure might arise if the cluster gas is polytropic, so that

$$f_T \propto f_n^{\gamma-1}. \quad (4.12)$$

The X-ray spectrum of Abell 665 does permit $\gamma \neq 1$, although the best-fitting atmosphere is isothermal. For any particular value of γ , and assuming that f_n takes the form of equation (3.14), it is simple to recalculate the angular structure variables $\Theta^{(1)}$ and $\Theta^{(2)}$ and to perform new fits for N_{RJ} and N_X . Equation (3.12) for the angular diameter distance, D_A , continues to apply, and it is easy, therefore, to recalculate the implied value of the Hubble constant. None of the polytropic models considered by Hughes & Tanaka (1991) that are acceptable fits to the X-ray spectrum at the 90% confidence level cause variations in the estimate of the Hubble constant by a factor as large as 1.5.

If extremely nonisothermal atmospheres are permitted as models of Abell 665, large variations in the result for the Hubble constant can be produced. If attention is restricted to polytropic β -models (where the density structure follows eq. [3.14], and the temperature is related to the density by eq. [4.11]), stronger limits to the model dependence of the Hubble constant can be imposed based on the goodness of fit of the X-ray image, the X-ray spectrum, and the Sunyaev-Zel'dovich effect, and we estimate that only about a 50% variation in H_0 is likely from such structures in the X-ray-emitting gas. However, resolved X-ray spectroscopy of Abell 665, and X-ray imaging of the faint outer parts of the cluster, are needed to probe the thermal structure of the cluster and control this possible source of error in the Hubble constant.

4.5. Contaminating X-Ray and SZ Signals

The X-ray spectrum, the X-ray image, and the Sunyaev-Zel'dovich effect scan across Abell 665 may all be contaminated by effects not connected with the gas in the cluster. If the level of such contaminations is large, then the values of N_X , N_{RJ} , and T_{e0} used in equation (3.12) may be incorrect.

The X-ray spectrum of the cluster is slightly contaminated by emission from point sources near the cluster center. Figure 2 demonstrates that several faint X-ray point sources lie within the FWHM of the *Ginga* spectrometer. If these sources have flat spectra, then they might cause an overestimation of the temperature of the cluster atmosphere (and hence an overestimation of the value of the Hubble constant)—but the contribution of these sources to the total cluster X-ray flux is only a few per cent at 6 keV, so that their effect on the cluster spectrum will be negligible (Hughes & Tanaka 1991). An alternative source of power-law X-ray emission might be from inverse-Compton emission by the radio halo source in Abell 665 (Moffet & Birkinshaw 1989). However, the location and angular structure of the radio halo is inconsistent with a large fraction of the extended cluster X-ray emission arising from this cause. We conclude that the X-ray spectrum provides a reliable estimate of the spectrum of the X-ray gas in the cluster.

Again, the X-ray structure of Abell 665 might be somewhat affected by the presence of emission from the radio halo source—but this effect, if present, can have only a small effect on the value of N_X —no emission that can be directly associ-

ated with the halo source can be seen on the HRI or IPC fields. The fitted value of N_X may also be affected by the gaseous halos of galaxies in the cluster—their gas contents need have no direct relationship to the density of the intracluster gas, and yet they will contribute to the integrated X-ray surface brightness of the cluster. However, such contributions should be restricted to the lower energy X-rays emitted by the cluster, and so only a small effect on the normalization and spectrum fitted should result. In future work, it might be desirable to minimize this effect by working with imaging and spectral data at energies greater than 3 keV, or to eliminate such point sources from the data by using high-resolution, high-sensitivity, X-ray images such as will be obtained by *AXAF*.

The radio halo source in Abell 665 is certainly responsible for “filling in” some of the Sunyaev-Zel’dovich effect in the cluster, but this effect has been largely subtracted by the radio source correction applied to the Sunyaev-Zel’dovich effect data (see § 2.1), and is small because of the steep radio spectrum of radio halo sources. Cool gas lying in a shell around the cluster will tend to mimic the Sunyaev-Zel’dovich effect, and could lead to an overestimation of the value of N_{RJ} . However, such a gas shell would be unstable, and should be seen in the scan (Fig. 1) as an excess of emission near the outer points. Its absence suggests that the effects of cool gas are less than the error in the zero level of the scan and may be ignored.

An effect that cannot be ignored in such a way is the effect of the motion of the cluster with respect to the Hubble flow. If the cluster has a peculiar velocity v along the line of sight, relative to the Hubble flow, then an anisotropy proportional to the Sunyaev-Zel’dovich effect, but smaller by a factor $\approx 0.9(v/10^3 \text{ km s}^{-1})(T_e/\text{keV})^{-1}$ at low frequencies, is introduced into the microwave background radiation. The quantity N_{RJ} fitted from the scan across the cluster must include a contribution from this effect—if $v \approx 10^3 \text{ km s}^{-1}$, then this could be as much as $\pm 10\%$ of the total signal. In this case, then the angular diameter distance may have been over or underestimated by 20%, and the Hubble constant may have been over or underestimated by 20%.

A direct measurement of this effect may be obtained from the frequency dependence of the apparent Sunyaev-Zel’dovich effect from Abell 665—but spectral measurements of the Sunyaev-Zel’dovich effect are likely to be difficult. Alternatively, the velocity effect can be regarded as merely a contribution to the scatter of the Hubble diagram deduced from equation (3.12)—and the effects of the cluster velocities can be averaged out by repeating this method for a number of clusters of galaxies.

4.6. Abell 2218

McHardy et al. (1990) have recently applied this same method to the cluster Abell 2218, from which they deduced $H_0 = 24_{-10}^{+13} \text{ km s}^{-1} \text{ Mpc}^{-1}$. This result is somewhat different from our result (eq. [3.19]) for the Hubble constant deduced from the data for Abell 665. Does this difference reflect the intrinsic uncertainty in the method for the derivation of H_0 , statistical variation, or some problem with the data on one or the other of these clusters?

It is certainly clear that Abell 665 and Abell 2218 are quite different clusters in their gas properties. Abell 665 has a gas temperature of more than 8 keV, whereas Abell 2218 is cooler, with a temperature of less than 7 keV. Abell 665 has a well-resolved Sunyaev-Zel’dovich effect, whereas the Sunyaev-

Zel’dovich effect in Abell 2218 is essentially unresolved, despite lying at a similar distance to Abell 665 (Birkinshaw 1990).

These data have the interesting consequence that while the X-ray image and Sunyaev-Zel’dovich scan for Abell 665 are consistent with a simple, isothermal atmosphere, this appears not to be the case for Abell 2218—the Sunyaev-Zel’dovich effect should have a larger angular extent than is observed. In their calculation of the Hubble constant, McHardy et al. (1990) use a value for N_{RJ} for Abell 2218 deduced on the assumption that the cluster is isothermal and follows equation (3.12) in its density distribution, with $\beta = 0.5$ and $\theta_C = 1.0$. They then combine this value of N_{RJ} with values for n_e and T_e deduced by *deconvolving* the HRI image of the cluster in order to deduce H_0 , making the assumptions that the gas is isothermal or adiabatic to relate n_e and T_e . Thus their application of the method compares models of the X-ray and Sunyaev-Zel’dovich structures of the cluster gas which are not necessarily consistent, and we should not expect the correct result for the Hubble constant (whatever it is) to emerge. Indeed, preliminary calculations suggest that this inconsistency may account for an error of a factor ≈ 2 in their estimate of the Hubble constant (Birkinshaw & Hughes 1991).

The calculation of the Hubble constant based on the X-ray and Sunyaev-Zel’dovich effect data for Abell 2218 should be repeated using consistent descriptions of the density and thermal structure of the gas and with more rigorous consideration of the level of systematic errors in the Sunyaev-Zel’dovich effect (particularly the zero-level errors, which presumably dominate the systematic error in the Hubble constant deduced from Abell 2218 just as they do for Abell 665). Such a calculation is presently in progress (Birkinshaw & Hughes 1991). From the discussion earlier in § 4, it is clear that errors in the description of the cluster atmosphere can give variations of factors ≈ 2 in the value of the Hubble constant that is calculated. A low estimate for the Hubble constant may be appropriate for any given cluster because of an intrinsically prolate atmosphere (§ 4.1), a significant velocity relative to the Hubble flow (§ 4.5), or a hot, low-density component to the cluster atmosphere (§ 4.4). Indeed, the selection effects in the use of Abell 665 and Abell 2218 as distance indicators may bias to low values the estimate of the Hubble constant derived using this method (§ 4.1).

5. CONCLUSIONS

The conclusions of this work can be summarized as follows.

1.—Adopting the simplest model atmosphere for Abell 665, and fitting this model to the X-ray and Sunyaev-Zel’dovich effect data, an estimate of the Hubble constant with good formal (statistical) errors can be obtained. The overall result is

$$H_0 = (40 \text{ to } 50) \pm 12 \text{ km s}^{-1} \text{ Mpc}^{-1}, \quad (5.1)$$

where the range expresses the maximum range of systematic errors associated with the zero level uncertainty in the Sunyaev-Zel’dovich effect, and the random and other systematic errors have been combined in quadrature. If the systematic errors are added directly, to obtain a worst case estimate of the errors, the result becomes

$$H_0 = (26 \pm 8) \text{ to } (65 \pm 10) \text{ km s}^{-1} \text{ Mpc}^{-1}. \quad (5.2)$$

2.—The random error estimates are dominated by the uncertainty in the temperature of the cluster gas and in the size of the central Sunyaev-Zel’dovich effect. The principal

improvement in the random errors would be achieved by obtaining high-precision X-ray spectra of the cluster, and by making high-sensitivity Sunyaev-Zel'dovich effect maps with higher angular resolution (to increase the beam-smearing Sunyaev-Zel'dovich effect signal).

3.—The systematic errors are dominated by the remaining uncertainty in the zero level of the Sunyaev-Zel'dovich effect data: the presence of a small “baseline” signal in the data of Fig. 1 would have a significant effect on the fitted central Sunyaev-Zel'dovich decrement, and hence a major effect on the H_0 estimate. A two-dimensional map of the Sunyaev-Zel'dovich effect should provide much more baseline information, and reduce this uncertainty further.

4.—After these errors in the data are dealt with, there would remain further serious difficulties with the method caused by the simplicity of the model used for the cluster atmosphere (i.e., our ignorance of the detailed structure of cluster atmospheres). For any single cluster, the intrinsic three-dimensional figure is unknown, and a systematic error of up to a factor 2 in either sense in the derived value of H_0 may result. A complete sample of clusters must be observed to eliminate this effect (and that sample must be selected without regard to the central brightnesses of its members, to avoid biasing the sample with prolate objects). Clumping of the intracluster medium will also bias the value of H_0 : if the cluster contains isothermal clumps, then the value for H_0 is an overestimate. Finally, if the gas distribution in the cluster does not smoothly connect the regions which contribute most of the X-ray emissivity (the central part of the cluster) and most of the Sunyaev-Zel'dovich effect (more diffuse regions, at larger radii), then it will be difficult to relate the X-ray and Sunyaev-Zel'dovich effect *integrated across the*

cluster, and the estimate for H_0 based upon simple density and temperature models (such as eq. [3.14]) will be inappropriate. Extremely sensitive X-ray images of clusters are needed to follow the cluster gas out to radii that contain most of the Sunyaev-Zel'dovich effect.

Despite these difficulties, it is encouraging that estimate (5.1) for the Hubble constant is not very different from the canonical values of 50 or 100 km s⁻¹ Mpc⁻¹. This may be fortuitous, with some of the effects mentioned above canceling—for example if Abell 665 is a clumpy, prolate, object—or it may indicate that the atmosphere of Abell 665 is sufficiently smooth and simple for this method to be applied. Whether or not this is true, it is clear that a further test of the method requires its application to several other clusters, to see whether the estimates for the Hubble constant deduced from their properties are consistent with estimate (5.1). Further work is also needed for Abell 665, to check the consistency of the physical description of the cluster atmosphere through higher sensitivity X-ray imaging and observations of the distribution and velocity dispersion of the cluster galaxies. Some theoretical work on the types of clumping that can survive in the cluster environment would also be helpful in eliminating some of the uncertainties in the description of the cluster environment.

This work was partially supported by the National Science Foundation under grant AST-9005038 to M. B., the Sloan Foundation through a Research Fellowship to M. B., the NASA *Ginga* Visiting Investigator Program through grant NAG8-699 to J. P. H., and Harvard University through research funds. The Government has certain rights in this material.

REFERENCES

- Aaronson, M., Bothun, G., Mould, J., Huchra, J., Schommer, R. A., & Cornell, M. E. 1986, *ApJ*, 302, 536
 Abell, G. O. 1958, *ApJS*, 3, 211
 Abramopoulos, F., & Ku, W. H.-M. 1983, *ApJ*, 271, 446
 Arnaud, K. A. 1991, in preparation
 Bartel, N. 1985, in *Supernovae as Distance Indicators*, ed. N. Bartel (Lecture Notes in Physics, Vol. 224) (Berlin: Springer), 107
 Birkinshaw, M. 1979, *MNRAS*, 187, 847
 ———. 1990, in *The Cosmic Microwave Background: 25 Years Later*, ed. N. Mandolesi & N. Vittorio (Dordrecht: Kluwer), 77
 Birkinshaw, M., & Gull, S. F. 1984, *MNRAS*, 206, 359
 Birkinshaw, M., Gull, S. F., & Hardebeck, H. E. 1984, *Nature*, 309, 34
 Birkinshaw, M., Gull, S. F., Hardebeck, H. E., & Moffet, A. T. 1991, in preparation
 Birkinshaw, M., Gull, S. F., & Moffet, A. T. 1981, *ApJ*, 251, L69
 Birkinshaw, M., Gull, S. F., & Northover, K. J. E. 1981, *MNRAS*, 197, 571
 Birkinshaw, M., & Hughes, J. P. 1991, in preparation
 Birkinshaw, M., & Moffet, A. T. 1986, *Highlights Astr.*, 7, 321
 Boynton, P. E., Radford, S. J. E., Schommer, R. A., & Murray, S. S. 1982, *ApJ*, 257, 473
 Branch, D. 1985, in *Supernovae as Distance Indicators*, ed. N. Bartel (Lecture Notes in Physics, Vol. 224) (Berlin: Springer), 138
 Carter, D., & Metcalfe, N. 1980, *MNRAS*, 191, 325
 Cavaliere, A., Danese, L., & De Zotti, G. 1979, *A&A*, 75, 322
 Cavaliere, A., & Fusco-Femiano, R. 1976, *A&A*, 49, 137
 ———. 1978, *A&A*, 70, 667
 de Vaucouleurs, G., & Corwin, H. G. 1986, *ApJ*, 308, 487
 Dressler, A. 1978a, *ApJ*, 223, 765
 ———. 1978b, *ApJ*, 226, 55
 Dressler, A., Lynden-Bell, D., Burstein, D., Davies, R. L., Faber, S. M., Terlevich, R. J., & Wegner, G. 1987, *ApJ*, 313, 42
 Edge, A. C., Stewart, G. C., Fabian, A. C., & Arnaud, K. A. 1990, *MNRAS*, 245, 559
 Forman, W., & Jones, C. 1982, *ARA&A*, 20, 547
 Gaillardetz, R., Bjorkholm, P., Mastronardi, R., Vanderhill, M., & Howland, D. 1978, *IEEE Trans.*, NS-25, 459
 Geller, M. J., & Beers, T. C. 1982, *PASP*, 94, 421
 Giacconi, R., et al. 1979, *ApJ*, 230, 540
 Gioia, I. M., Maccacaro, T., Schild, R. E., Wolter, A., Stocke, J. T., Morris, S. L., & Henry, J. P. 1990, *ApJS*, 72, 567
 Gull, S. F., & Northover, K. J. E. 1976, *Nature*, 263, 572
 Gunn, J. E. 1978, in *Observational Cosmology*, ed. A. Maeder, L. Martinet, & G. Tammann (Sauverny: Geneva Observatory), 1
 Hayashida, K., et al. 1989, *PAS Japan*, 41, 373
 Henry, J. P., & Henriksen, M. J. 1986, *ApJ*, 301, 689
 Hughes, J. P., & Tanaka, Y. 1991, *ApJ*, submitted
 Hughes, J. P., Yamashita, K., Okamura, Y., Tsunemi, H., & Matsuoka, M. 1988, *ApJ*, 327, 615
 Jones, C., Mandel, E., Schwarz, J., Forman, W., Murray, S. S., & Harnden, F. R., Jr. 1979, *ApJ*, 234, L21
 Kogut, A., et al. 1988, *ApJ*, 325, 1, and erratum 332, 1092
 Krolik, J. H., & Raymond, J. C. 1988, *ApJ*, 335, L39
 Lake, G., & Partridge, R. B. 1980, *ApJ*, 237, 378
 Lynden-Bell, D. 1977, *Nature*, 270, 396
 McHardy, I. M., Stewart, G. C., Edge, A. C., Cooke, B., Yamashita, K., & Hatsukade, I. 1990, *MNRAS*, 242, 215
 Moffet, A. T., & Birkinshaw, M. 1989, *AJ*, 98, 1148
 Press, W. H., Flannery, B. P., Teukolsky, S. A., & Vetterling, W. T. 1986, in *Numerical Recipes* (Cambridge: Cambridge University Press), 539
 Raymond, J. C., & Smith, B. W. 1977, *ApJS*, 35, 419
 Readhead, A. C. S., Lawrence, C. R., Myers, S. T., Sargent, W. L. W., Hardebeck, H. E., & Moffet, A. T. 1989, *ApJ*, 346, 566
 Sargent, W. L. W. 1973, *PASP*, 85, 281
 Sastry, G. N., & Rood, H. J. 1971, *ApJS*, 23, 371
 Silk, J. I., & White, S. D. M. 1978, *ApJ*, 226, L103
 Tammann, G. A., & Sandage, A. 1983, *Highlights Astr.*, 6, 301
 Tully, R. B. 1988, *Nature*, 334, 209
 Uson, J. M. 1986, in *Radio Continuum Processes in Clusters of Galaxies*, ed. C. P. O'Dea & J. M. Uson (Green Bank: NRAO), 255
 van den Bergh, S. 1988, in *The Extragalactic Distance Scale*, ed. S. van den Bergh & C. J. Pritchett (San Francisco: Astronomical Society of the Pacific), 221
 White, S. D. M., & Silk, J. I. 1980, *ApJ*, 248, 864
 White, S. D. M., Silk, J. I., & Henry, J. P. 1981, *ApJ*, 251, L65